

## 5.2 Load Combinations and Allowable Stress Intensities

The stress ratios computed for CLTP at nominal frequency and with frequency shifting are listed in Table 9. The stress ratios are grouped according to type (SR-P for maximum membrane and membrane+bending stress, SR-a for alternating stress) and location (away from welds or on a weld). The tabulated nodes are also depicted in Figure 14 (no frequency shift) and Figure 15 (all frequency shifts included). The plots corresponding to maximum stress intensities depict all nodes with stress ratios less than 4 or 5 as indicated, and the plots of alternating stress ratios display all nodes with  $SR-a \leq 5$ .

For CLTP operation at nominal frequency the minimum stress ratio is identified as a maximum stress,  $SR-P=1.34$ , and is recorded on the bottom of the vertical plate joining the innermost vane banks. However, this location is only weakly responsive to acoustic loads as can be seen from the high alternating stress ratio at this location ( $SR-a > 16.5$  at all frequency shifts). This is true for all three nodes having the lowest values of SR-P, all having  $SR-a > 5.1$  at all frequency shifts. The minimum alternating stress ratio at zero frequency shift,  $SR-a=3.00$ , occurs on the weld connecting the inner hood and hood support.

The effects of frequency shifts can be conservatively accounted for by identifying the minimum stress ratio at every node, where the minimum is taken over all the frequency shifts considered (including the nominal or 0% shift case). The resulting stress ratios are then processed as before to identify the smallest stress ratios anywhere on the structure, categorized by stress type (maximum or alternating) and location (on or away from a weld). The results are summarized in Table 9b and show that the lowest stress ratio,  $SR-P=1.34$ , occurs at the same location as in the nominal case and retains virtually the same value. Moreover, the next three lowest SR-P locations are the same as in Table 9a. The lowest alternating stress ratio,  $SR-a=2.89$  occurs at the common intersection point of the bottom of the inner hood, hood support and base plate (see Figure 15f). Hood supports are also involved in locations 3-5, 10-11 and 15. The next lowest SR-a location involves the lifting rod support brace (Figure 15g) involving locations 2 and 7. The remaining low alternating stress ratio locations occur on: (i) closure plates (locations 9 and 16); (ii) tie bar ends or their immediate vicinity (locations 12 and 14); or (iii) the hoods.

The estimated alternating stress ratio at EPU operation is obtained by scaling the corresponding value at CLTP by the square of the ratio of the steam flow velocities at EPU and CLTP conditions. Since this ratio,  $(U_{EPU}/U_{CLTP})^2=1.178^2=1.388$ , the limiting alternating stress ratio at any frequency shift for EPU is estimated as  $SR-a=2.89/1.388=2.08$ . This value qualifies the Unit 2 dryer at EPU conditions with considerable margin. The limiting stress ratio, SR-P, is dominated by the static load and has a weaker dependence on power. When this node is reanalyzed with the MSL signals increased by 1.388, the limiting SR-P reduces to 1.32 at EPU.

In summary, the lowest alternating stress ratio occurs at the base of the inner hood support where it is welded to the middle base plate and vertical vane bank support. Its value,  $SR-a=2.89$  at the -5% frequency shift indicates that stresses are well below allowable levels. The lowest stress ratio associated with a maximum stress is  $SR-P=1.34$  at CLTP. This value is dominated by the static component and is only weakly altered by acoustic loads (it reduces to 1.32 at EPU). Since acoustic loads scale roughly with the square of the steam flow, the limiting alternating

stress ratio at EPU reduces to 2.08, which given that the applied loads already account for all end-to-end biases and uncertainties, still contains ample margin for sustained EPU operation.

Table 9a. Locations with minimum stress ratios for CLTP conditions with no frequency shift. Stress ratios are grouped according to stress type (maximum – SR-P; or alternating – SR-a) and location (away from a weld or at a weld). Bold text indicates minimum stress ratio of any type on the structure. Locations are depicted in Figure 14.

Stress Ratio	Weld	Location	Location (in.)			node(a)	Stress Intensity (psi)			Stress Ratio	
			x	y	z		Pm	Pm+Pb	S <sub>alt</sub>	SR-P	SR-a
SR-P	No	1. Inner Side Plate	3.1	119	0.5	37229	7475	8836	460	2.26	26.86
	"	2. Thin Vane Bank Plate	-15.6	-118.4	0.6	2558	4759	5171	<250	3.55	>27
		3. Support/Seismic Block	10.2	123.8	-9.5	113286	4354	4354	1374	3.88	9.00
SR-a	No	Middle Hood	-68.9	69.6	41.6	31054	1717	2759	2728	9.19	4.53
<b>SR-P</b>	<b>Yes</b>	<b>1. Side Plate Ext/Inner Base Plate</b>	<b>16.3</b>	<b>119</b>	<b>0</b>	<b>94143</b>	<b>6913</b>	<b>9809</b>	<b>438</b>	<b>1.34</b>	<b>15.67</b>
"	"	2. Upper Support Ring/Support/Seismic Block	-6.9	-122.3	-9.5	113554	6238	6238	911	1.49	7.54
"	"	3. Tie Bar	49.3	108.1	88	141275	5962	5962	807	1.56	8.51
"	"	4. Hood Support/Middle Base Plate/Inner Backing Bar/Inner Hood	39.9	-59.5	0	101435	5352	5488	1638	1.74	4.19
"	"	5. Inner Side Plate/Inner Base Plate	-2.3	-119	0	99200	4419	7921	511	1.76	13.44
"	"	6. Closure Plate/Inner Backing Bar Out/Inner Backing Bar/Inner Hood	39.9	108.6	0.5	93062	5232	5253	851	1.78	8.07
"	"	7. Hood Support/Outer Base Plate/Middle Backing Bar	-71.3	0	0	95428	4800	4876	1817	1.94	3.78
"	"	8. Side Plate/Top Plate	17.6	119	88	91215	898	7174	1337	1.94	5.14
"	"	9. Outer Cover Plate/Outer Hood	102.8	-58.1	0	94498	1020	7053	763	1.98	9.01
"	"	10. Hood Support/Middle Base Plate/Inner Backing Bar/Inner Hood <sup>(6)</sup>	-39.9	0	0	85723	4684	4849	1842	1.98	3.73
"	"	11. Thin Vane Bank Plate/Hood Support/Inner Base Plate	24.1	-59.5	0	85191	4385	4439	772	2.12	8.90

Notes.

- (a) Node numbers are retained for further reference.
- (1-9) Appropriate stress reduction factor for the welds and modifications listed in Table 7 have been applied. The number refers to the particular location and corresponding stress reduction factor in Table 7.

Table 9a (cont.). Locations with minimum stress ratios for CLTP conditions with no frequency shift. Stress ratios are grouped according to stress type (maximum – SR-P; or alternating – SR-a) and location (away from a weld or at a weld). Bold text indicates minimum alternating stress ratio on the structure. Locations are depicted in Figure 14.

Stress Ratio	Weld	Location	Location (in.)			node(a)	Stress Intensity (psi)			Stress Ratio	
			x	y	z		Pm	Pm+Pb	S <sub>alt</sub>	SR-P	SR-a
SR-a	Yes	1. Hood Support/Inner Hood	36.2	0	50.8	99529	975	2316	2290	6.02	3.00
"	"	2. Hood Support/Inner Hood	39.1	0	23	99515	842	2064	1977	6.75	3.47
"	"	3. Hood Support/Inner Hood	34.3	0	62.7	99535	826	2319	1970	6.01	3.49
"	"	4. Closure Plate/Middle Hood	-68.7	85.2	42.9	91590	693	1963	1936	7.10	3.55
"	"	5. Hood Support/Middle Hood	-68.7	54.3	42.9	99140	554	1968	1902	7.09	3.61
"	"	6. Side Plate/Brace <sup>(5)</sup>	-79.7	85.2	75.8	103160	1529	2892	1897	4.82	3.62
"	"	7. Hood Support/Inner Hood <sup>(7)</sup>	38	0	36.9	99522	741	1886	1860	7.39	3.69
"	"	8. Hood Support/Middle Base Plate/Inner Backing Bar/Inner Hood <sup>(6)</sup>	-39.9	0	0	85723	4684	4849	1842	1.98	3.73
"	"	9. Side Plate/Brace	79.7	85.2	31.2	89646	1447	2182	1820	6.39	3.77

Notes.

- (a) Node numbers are retained for further reference.
- (1-9) Appropriate stress reduction factor for the welds and modifications listed in Table 7 have been applied. The number refers to the particular location and corresponding stress reduction factor in Table 7.

Table 9b. Locations with minimum stress ratios for CLTP conditions with frequency shifts. Stress ratios at every node are recorded as the lowest stress ratio identified during the frequency shifts. Stress ratios are grouped according to stress type (maximum – SR-P; or alternating – SR-a) and location (away from a weld or at a weld). Bold text indicates minimum stress ratio of any type on the structure. Locations are depicted in Figure 15.

Stress Ratio	Weld	Location	Location (in.)			node(a)	Stress Intensity (psi)			Stress Ratio		% Freq. Shift
			x	y	z		Pm	Pm+Pb	S <sub>alt</sub>	SR-P	SR-a	
SR-P	No	1. Inner Side Plate	3.1	119	0.5	37229	7490	9003	634	2.26	19.51	10
"	"	2. Support/Seismic Block	10.2	123.8	-9.5	113286	4829	4829	2019	3.5	6.12	5
"	"	3. Thin Vane Bank Plate	-15.6	-118.4	0.6	2558	4792	5212	0	3.53	1360	2.5
SR-a	No	1. Middle Hood	-68.6	69.6	43.7	31149	1717	2953	2914	8.59	4.24	2.5
<b>SR-P</b>	<b>Yes</b>	<b>1. Side Plate Ext/Inner Base Plate</b>	<b>16.3</b>	<b>119</b>	<b>0</b>	<b>94143</b>	<b>6918</b>	<b>9809</b>	<b>478</b>	<b>1.34</b>	<b>14.38</b>	<b>5</b>
"	"	2. USR/Support/Seismic Block	-6.9	-122.3	-9.5	113554	6688	6688	1342	1.39	5.12	5
"	"	3. Tie Bar	-49.3	-108.1	88	143795	6077	6077	877	1.53	7.83	5
"	"	4. Hood Support/Middle Base Plate/Inner Backing Bar/Inner Hood	39.9	-59.5	0	101435	5495	5819	1815	1.69	3.78	-10
"	"	5. Closure Plate/Inner Backing Bar/Inner Backing Bar/Inner Hood	-39.9	-108.6	0.5	84198	5492	5499	1160	1.69	5.92	5
"	"	6. Inner Side Plate/Inner Base Plate	-2.3	-119	0	99200	4464	8176	793	1.71	8.66	5
"	"	7. Side Plate/Top Plate	17.6	119	88	91215	920	7332	1585	1.9	4.33	5
"	"	8. Hood Support/Outer Base Plate/Middle Backing Bar	-71.3	0	0	95428	4800	4876	1817	1.94	3.78	0
"	"	9. Outer Cover Plate/Outer Hood	102.8	-58.1	0	94498	1066	7197	910	1.94	7.55	10
"	"	10. Hood Support/Middle Base Plate/Inner Backing Bar/Inner Hood <sup>(6)</sup>	39.9	0	0	88639	4733	4874	1883	1.96	3.65	2.5
"	"	11. Thin Vane Bank Plate/Hood Support/Inner Base Plate	-24.1	59.5	0	99487	4707	4724	1091	1.97	6.3	10
"	"	12. Hood Support/Outer Cover Plate/Outer Hood <sup>(7)</sup>	-102.8	28.4	0	95267	4451	4533	1942	2.09	3.54	5

Notes.

(a) Node numbers are retained for further reference.

(1-9) Appropriate stress reduction factor for the welds and modifications listed in Table 7 have been applied. The number refers to the particular location and corresponding stress reduction factor in Table 7.

Table 9b (cont.). Locations with minimum stress ratios for CLTP conditions with frequency shifts. Stress ratios at every node are recorded as the lowest stress ratio identified during the frequency shifts. Stress ratios are grouped according to stress type (maximum – SR-P; or alternating – SR-a) and location (away from a weld or at a weld). Locations are depicted in Figure 15.

Stress Ratio	Weld	Location	Location (in.)			node(a)	Stress Intensity (psi)			Stress Ratio		% Freq. Shift
			x	y	z		Pm	Pm+Pb	S <sub>alt</sub>	SR-P	SR-a	
SR-a	Yes	1. Hood Support/Middle Base Plate/Inner Backing Bar/Inner Hood <sup>(6)</sup>	-39.9	0	0	85723	4695	4849	2378	1.98	2.89	-5
"	"	2. Side Plate/Brace <sup>(5)</sup>	79.7	85.2	75.8	89649	2002	2884	2343	4.64	2.93	10
"	"	3. Hood Support/Inner Hood	36.2	0	50.8	99529	975	2316	2290	6.02	3.00	0
"	"	4. Hood Support/Middle Base Plate/Inner Backing Bar/Inner Hood	-39.9	59.5	0	90468	5397	5524	2277	1.72	3.02	-5
"	"	5. Hood Support/Outer Hood	-96.4	-28.4	66.8	90186	657	2332	2234	5.98	3.07	5
"	"	6. Hood Reinforcement/Middle Hood	-62.6	101.2	77.9	98277	442	2408	2223	5.79	3.09	-10
"	"	7. Side Plate/Brace	-79.7	-85.2	31.2	84708	1818	2636	2175	5.11	3.16	2.5
"	"	8. Outer End Plate/Outer Hood	-97.5	-70	60.8	99212	802	2212	2165	6.30	3.17	5
"	"	9. Side Plate/Closure Plate/Exit Mid Bottom Perf	-78.5	-85.2	56.5	87780	524	2241	2147	6.22	3.20	7.5
"	"	10. Hood Support/Inner Backing Bar/Inner Hood	-39.9	0	1	95620	1943	3082	2100	4.52	3.27	-5
"	"	11. Hood Support/Inner Hood	34.3	0	62.7	99535	826	2451	2096	5.69	3.28	-10
"	"	12. Top Plate/Tie Bar	-17.6	-0.5	88	75048	1127	3064	2080	4.55	3.30	2.5
"	"	13. Top Thick Plate/Side Plate/Exit Top Perf/Inner Side Plate	-15.6	119	86.5	98451	816	2970	2070	4.70	3.32	2.5
"	"	14. Double Side Plate/Top Plate	-54	-54.3	88	85117	587	2323	2032	6.00	3.38	2.5
"	"	15. Hood Support/Outer Hood <sup>(7)</sup>	-97.8	-28.4	59	85774	488	2129	2027	6.55	3.39	5
"	"	16. Closure Plate/Middle Hood	-68.7	85.2	42.9	91590	710	2041	2022	6.83	3.40	2.5

(a) Node numbers are retained for further reference.

(1-9) Appropriate stress reduction factor for the welds and modifications listed in Table 7 have been applied. The number refers to the particular location and corresponding stress reduction factor in Table 7.

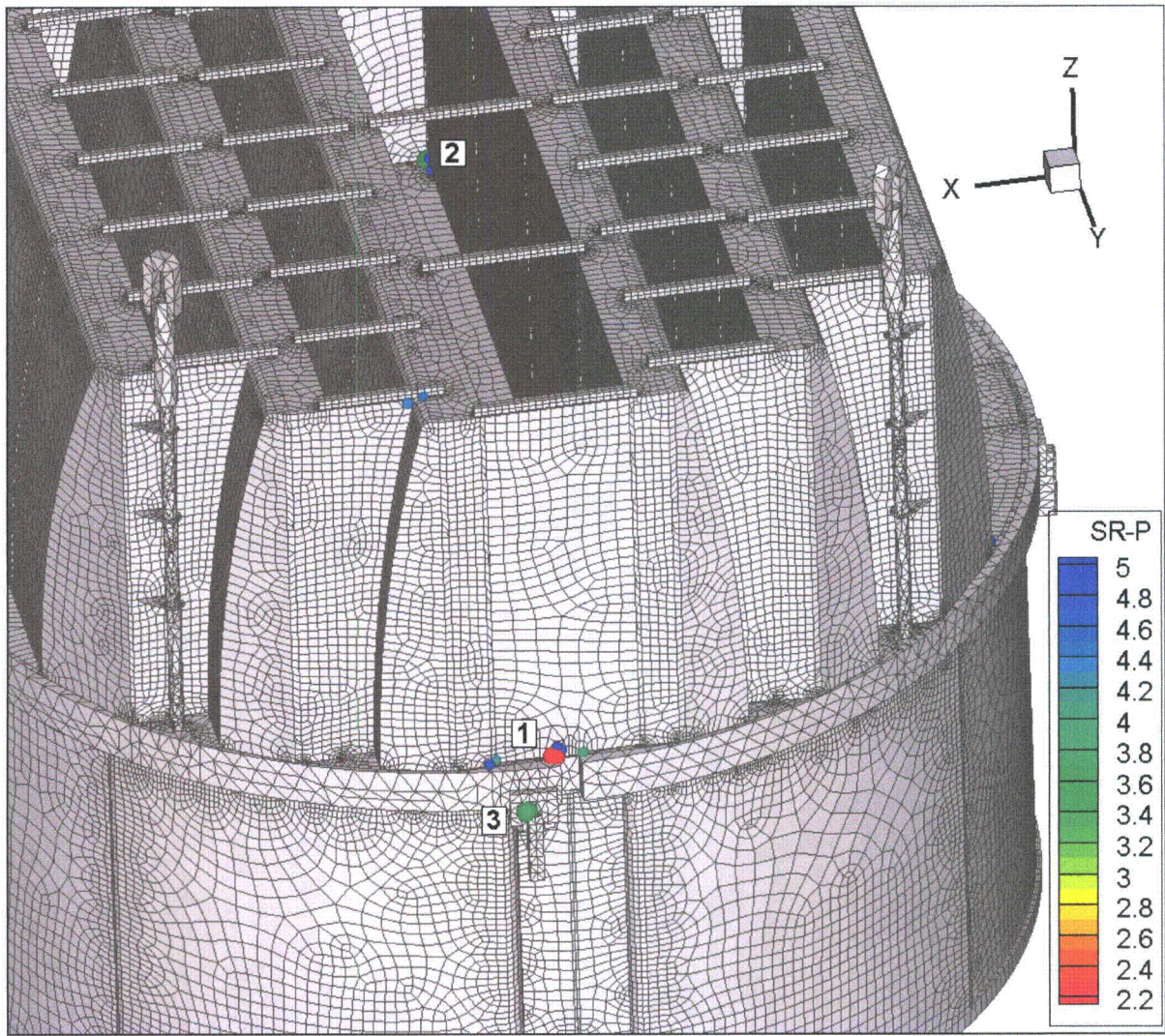


Figure 14a. Locations of nodes with stress ratios,  $SR-P \leq 5$ , associated with a maximum stress at non-welds for nominal CLTP operation. Numbers refers to the enumerated locations for SR-P values at non-welds in Table 9a.

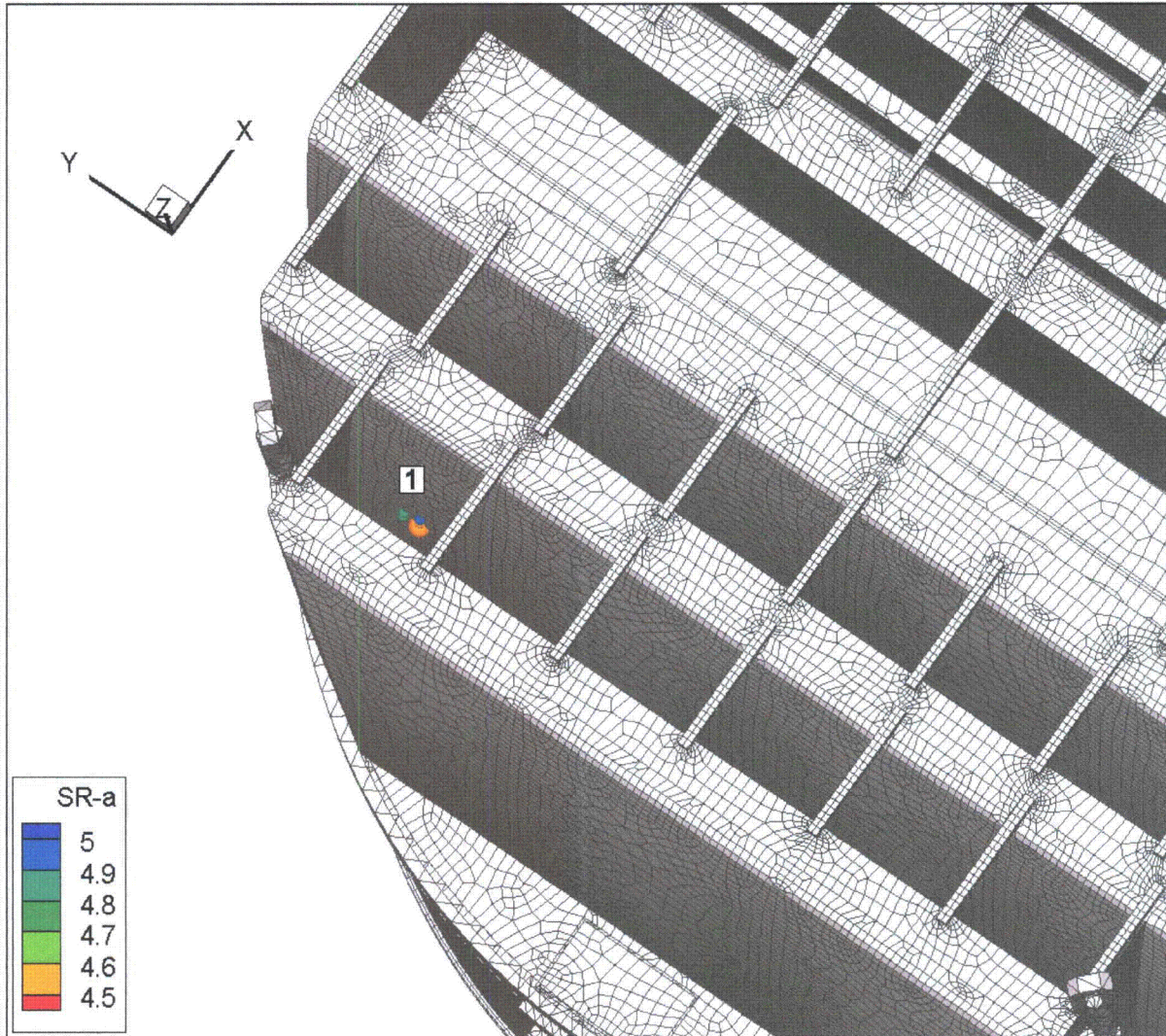


Figure 14b. Locations of smallest alternating stress ratios,  $SR-a \leq 5$ , at non-welds for nominal CLTP operation. Numbers refer to the enumerated locations for SR-a values at non-welds in Table 9a.

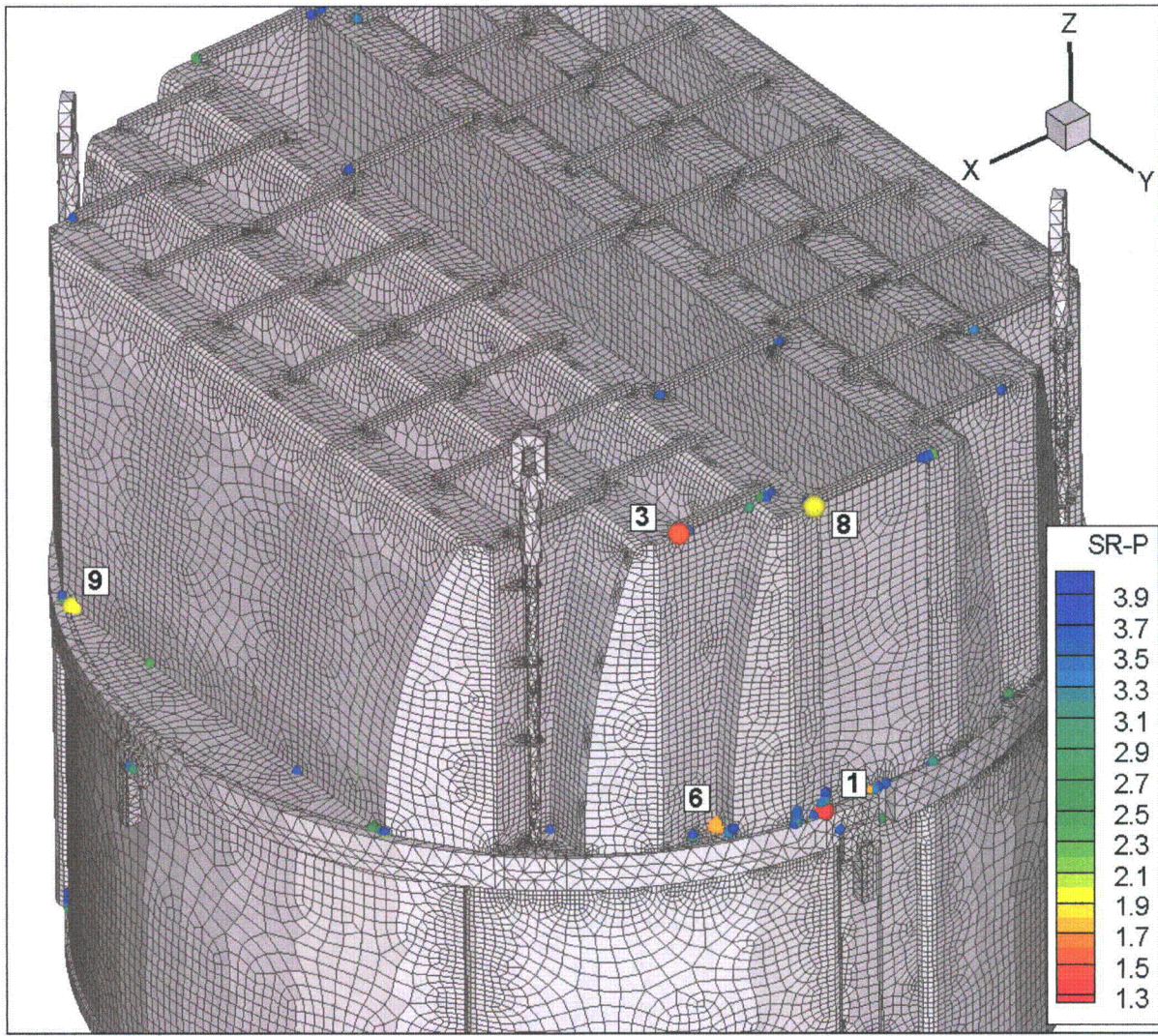


Figure 14c. Locations of smallest stress ratios,  $SR-P \leq 4$ , associated with maximum stresses at welds for nominal CLTP operation. Numbers refer to the enumerated locations for SR-P values at welds in Table 9a. This view shows locations 1, 3, 6, 8 and 9.

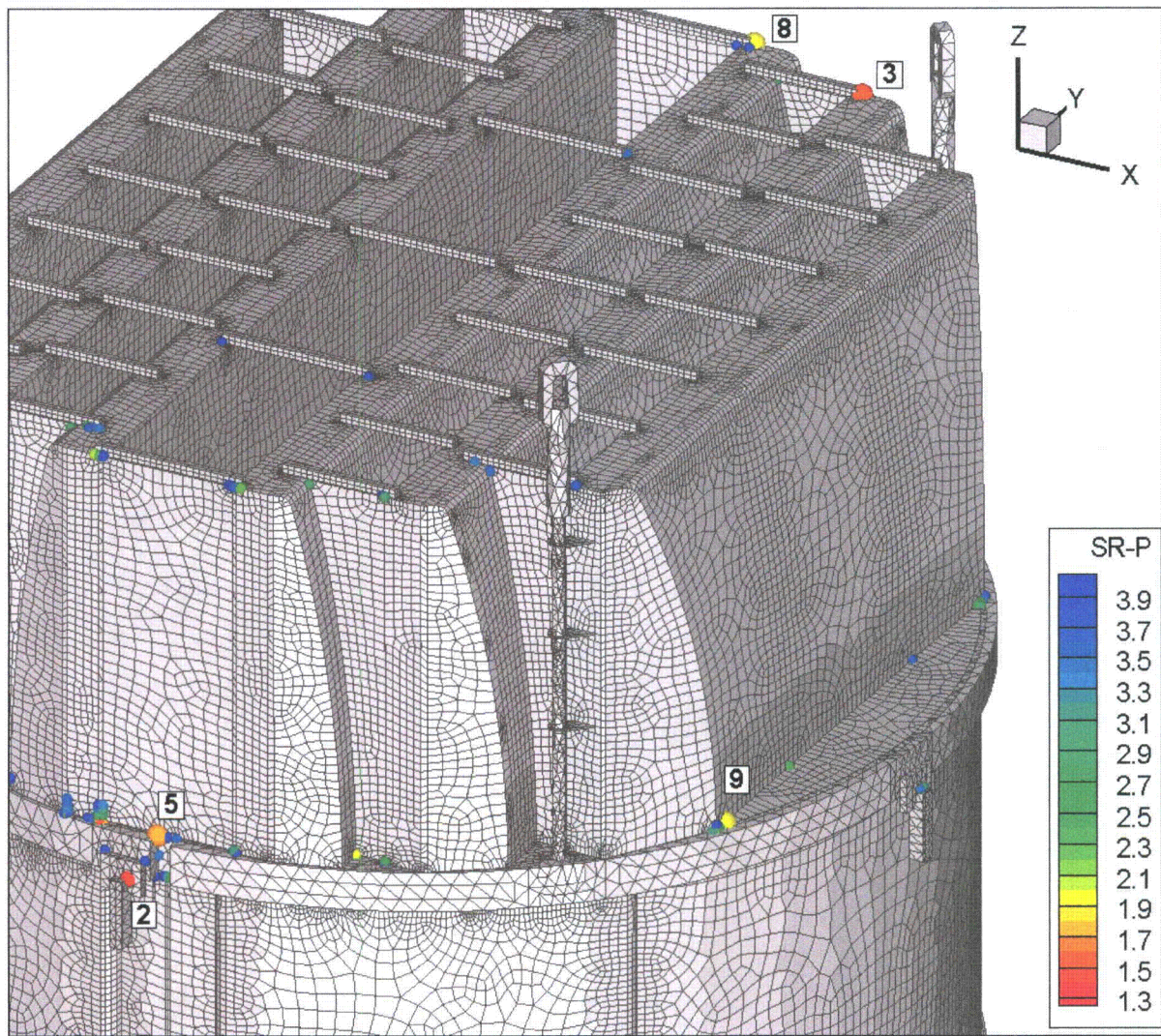


Figure 14d. Locations of minimum stress ratios,  $SR-P \leq 4$ , associated with maximum stresses at welds for nominal CLTP operation. Numbers refer to the enumerated locations for SR-P values at welds in Table 9a. This view shows locations 2, 3, 5, 8 and 9.

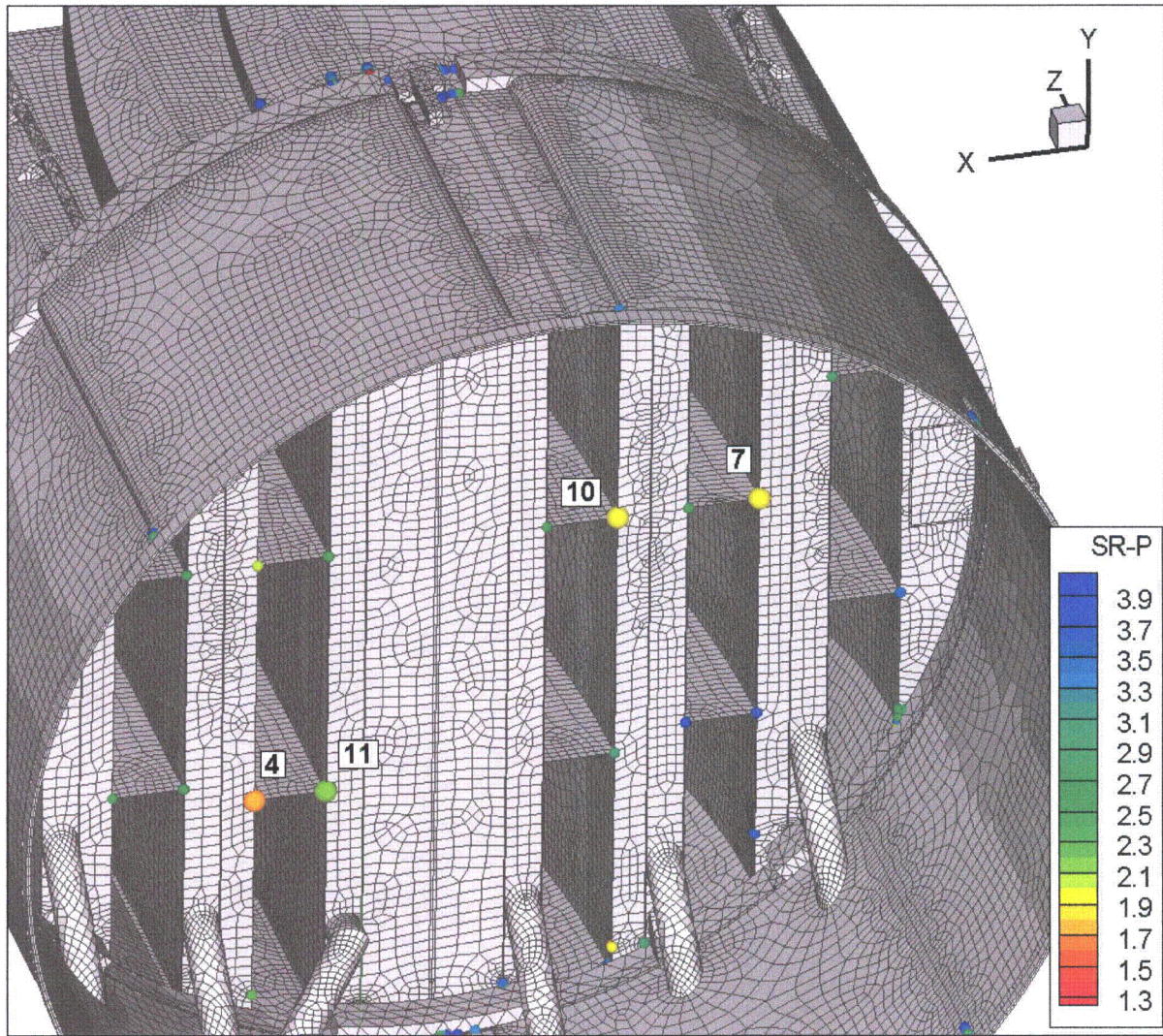


Figure 14e. Locations of minimum stress ratios,  $SR-P \leq 4$ , associated with maximum stresses at welds for nominal CLTP operation. Numbers refer to the enumerated locations for SR-P values at welds in Table 9a. This view shows locations 4, 7, 10 and 1

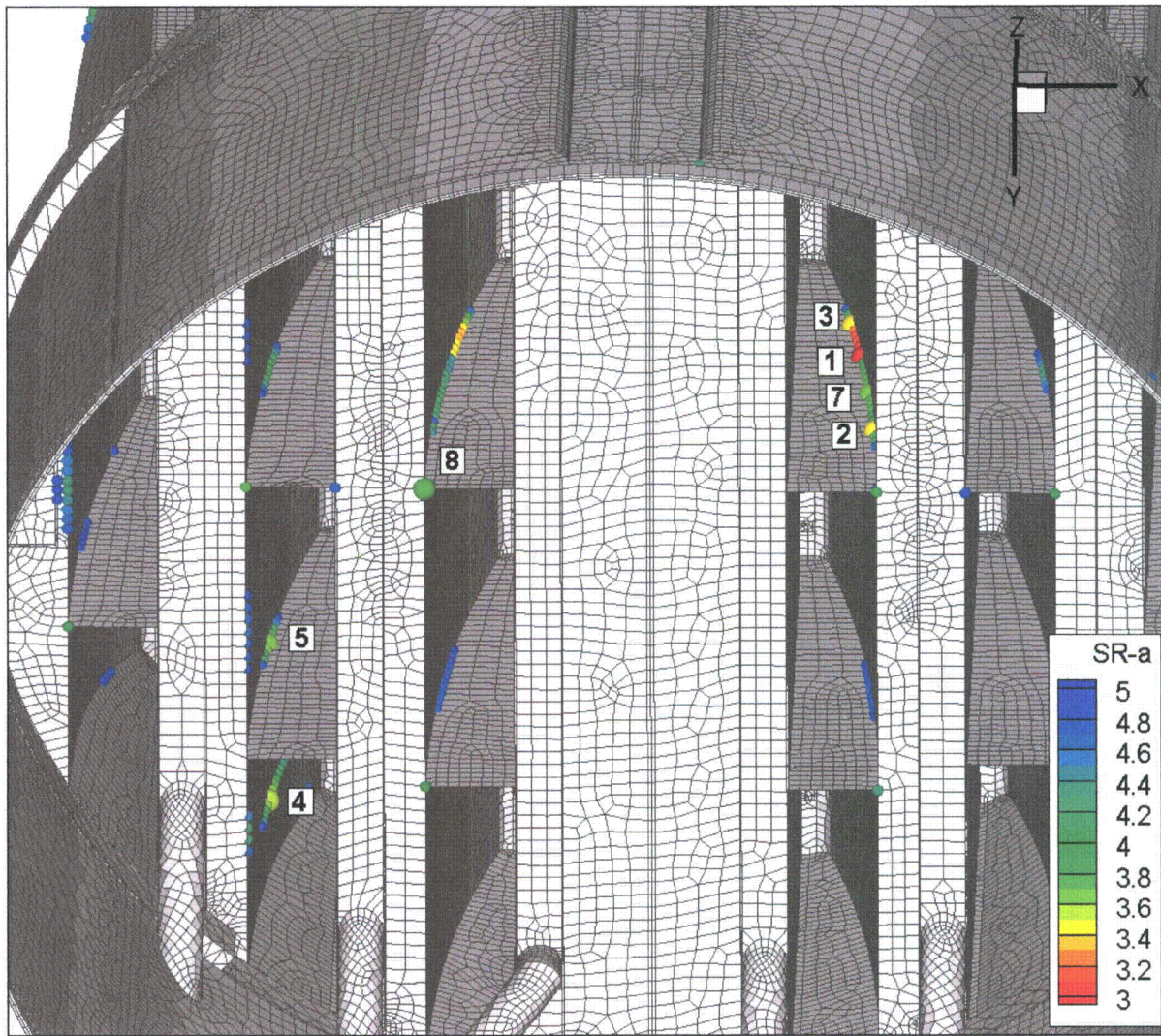


Figure 14f. Locations of minimum alternating stress ratios,  $SR-a \leq 5$ , at welds for nominal CLTP operation. Numbers refer to the enumerated locations for  $SR-a$  values at welds in Table 9a. Locations 1-5, 7 and 8 are shown.

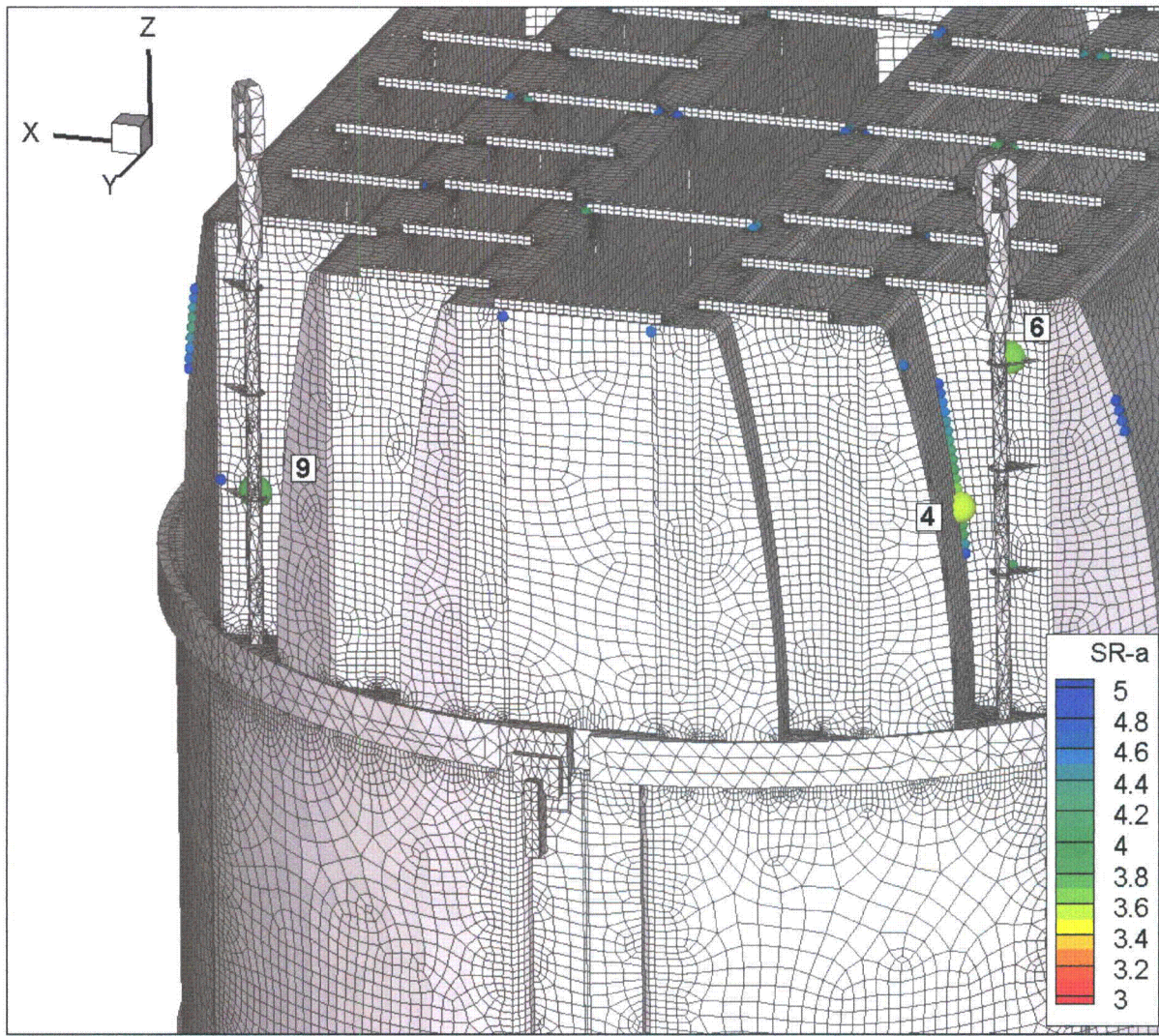


Figure 14g. Locations of minimum alternating stress ratios,  $SR-a \leq 5$ , at welds for nominal CLTP operation. Numbers refer to the enumerated locations for  $SR-a$  values at welds in Table 9a. Locations 4, 6 and 9 are shown.

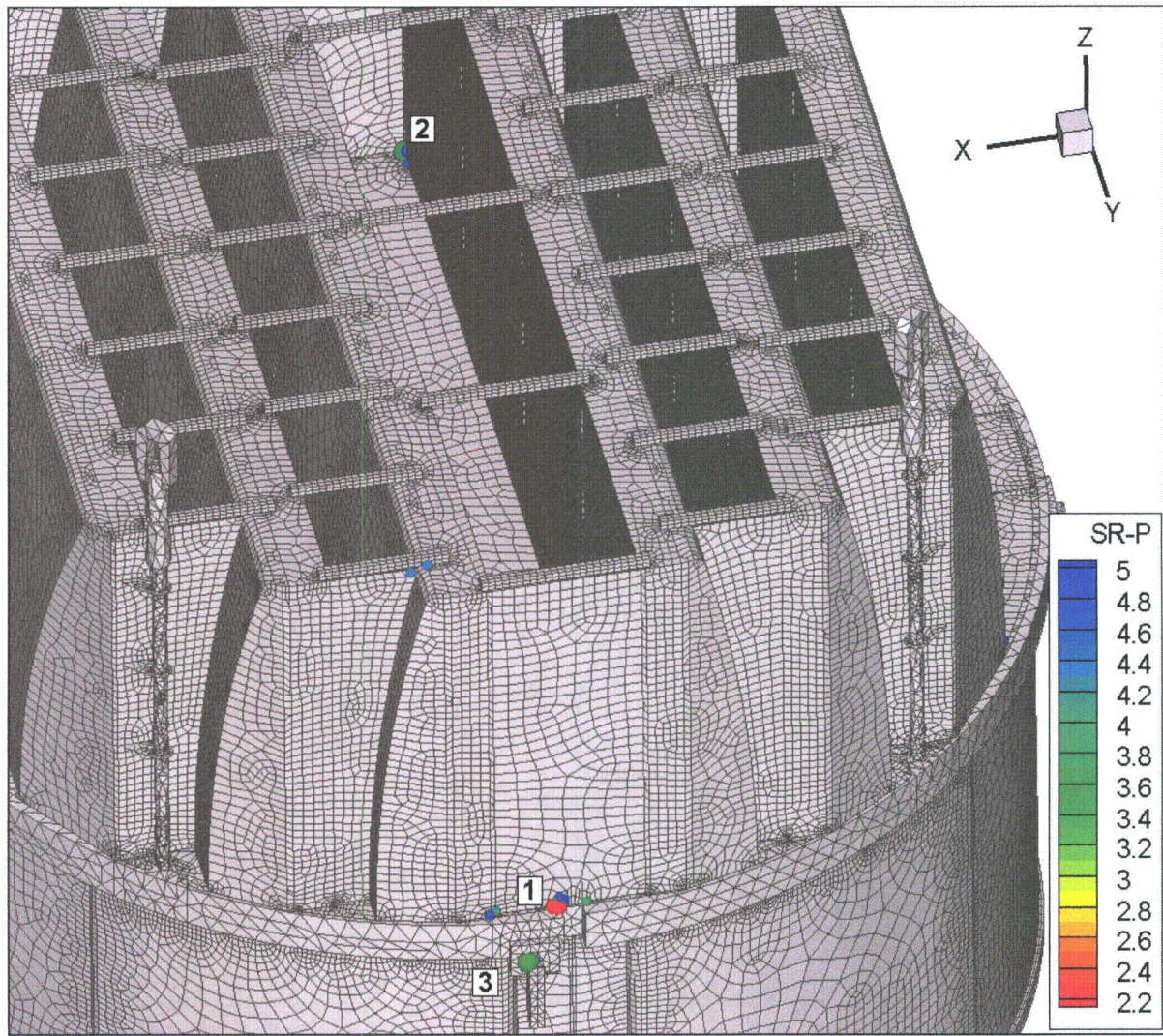


Figure 15a. Locations of minimum stress ratios,  $SR-P \leq 5$ , associated with maximum stresses at non-welds for CLTP operation with frequency shifts. The recorded stress ratio is the minimum value taken over all frequency shifts. The numbers refers to the enumerated location for SR-P values at non-welds in Table 9b.

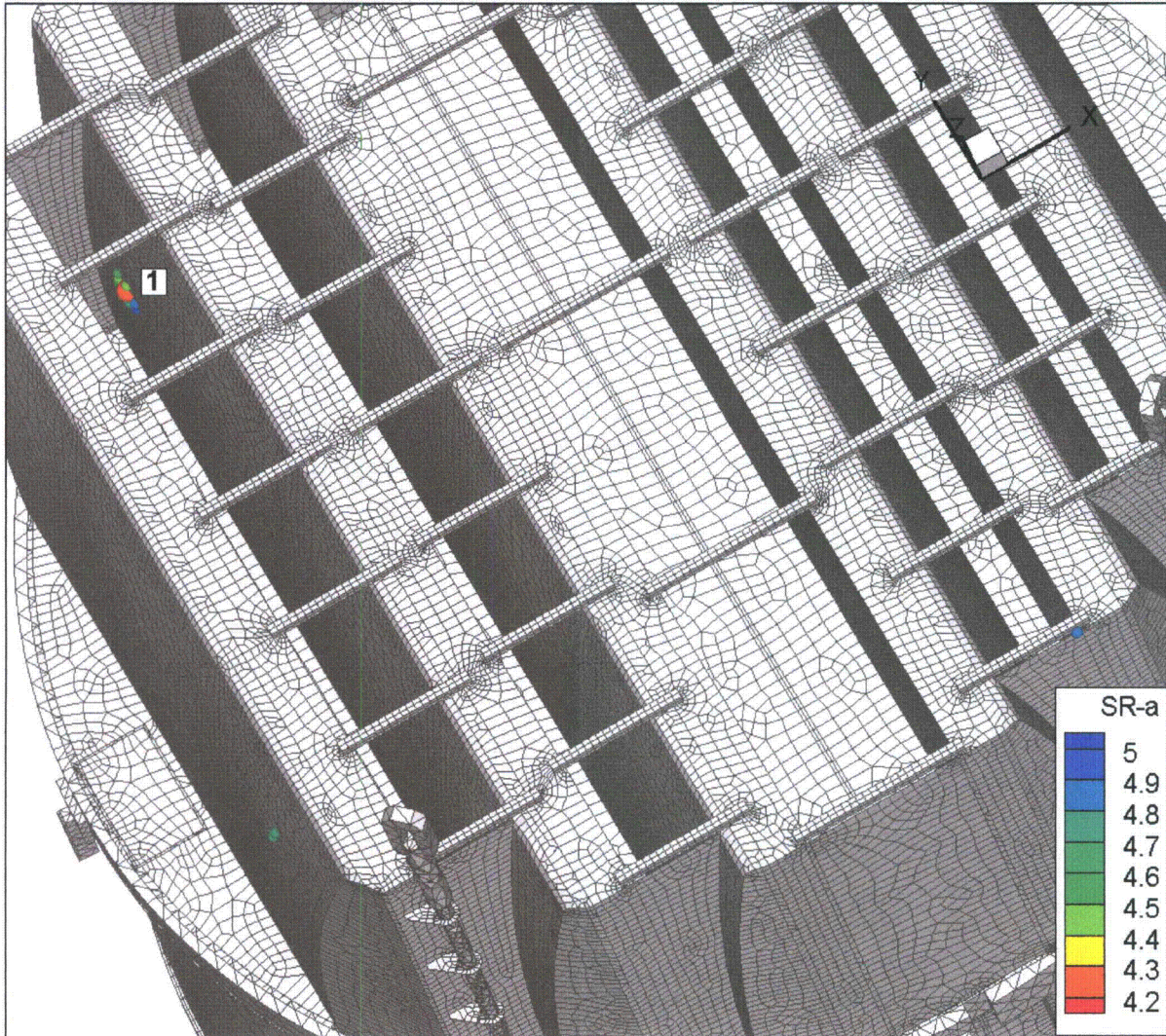


Figure 15b. Locations of minimum alternating stress ratios,  $SR-a \leq 5$ , at non-welds for CLTP operation with frequency shifts. The recorded stress ratio at a node is the minimum value taken over all frequency shifts. Numbers refer to the enumerated locations for SR-a values at non-welds in Table 9b.

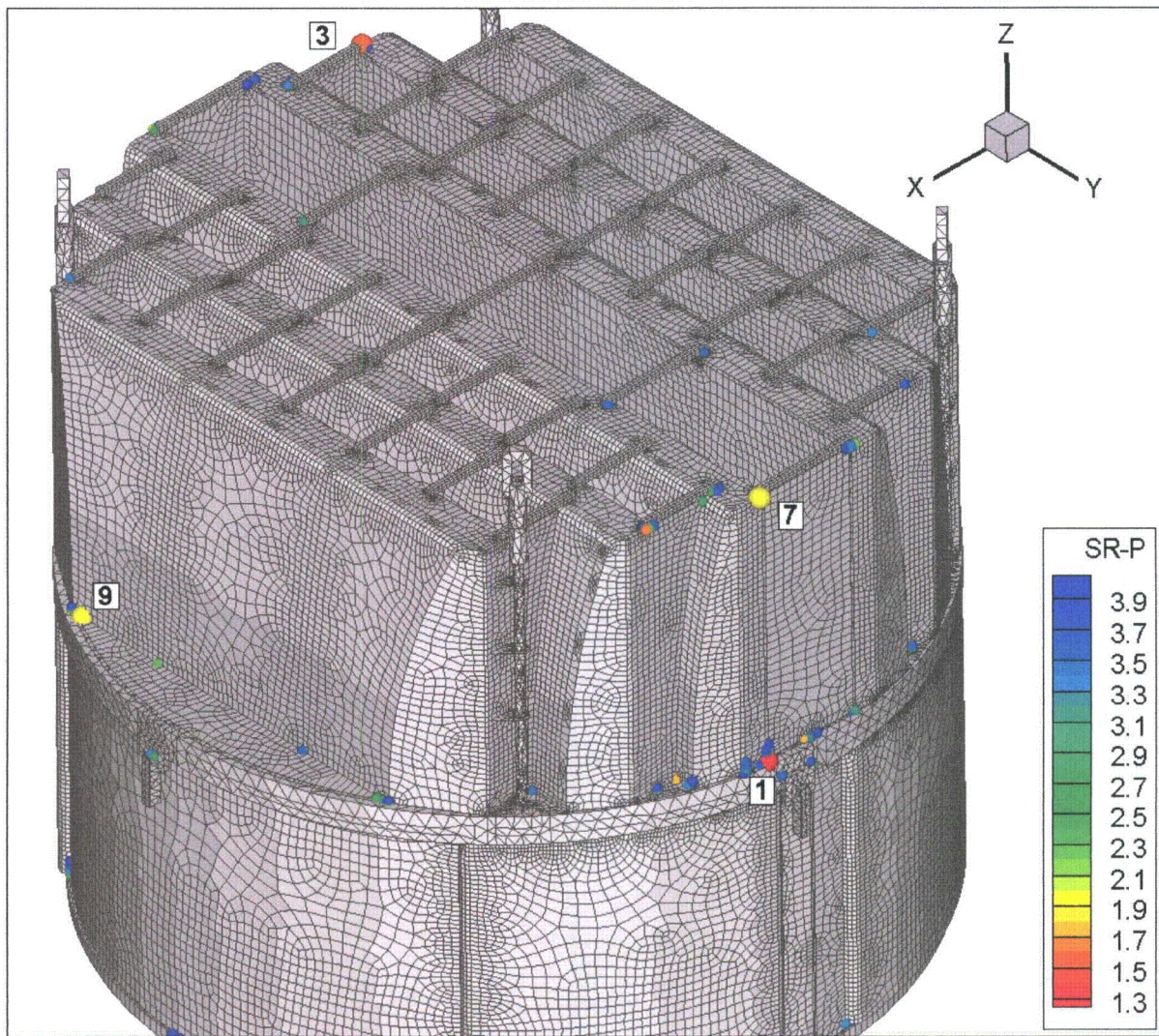


Figure 15c. Locations of minimum stress ratios,  $SR-P \leq 4$ , associated with maximum stresses at welds for CLTP operation with frequency shifts. The recorded stress ratio at a node is the minimum value taken over all frequency shifts. Numbers refer to the enumerated locations for SR-P values at welds in Table 9b. This view shows locations 1, 3, 7 and 9.

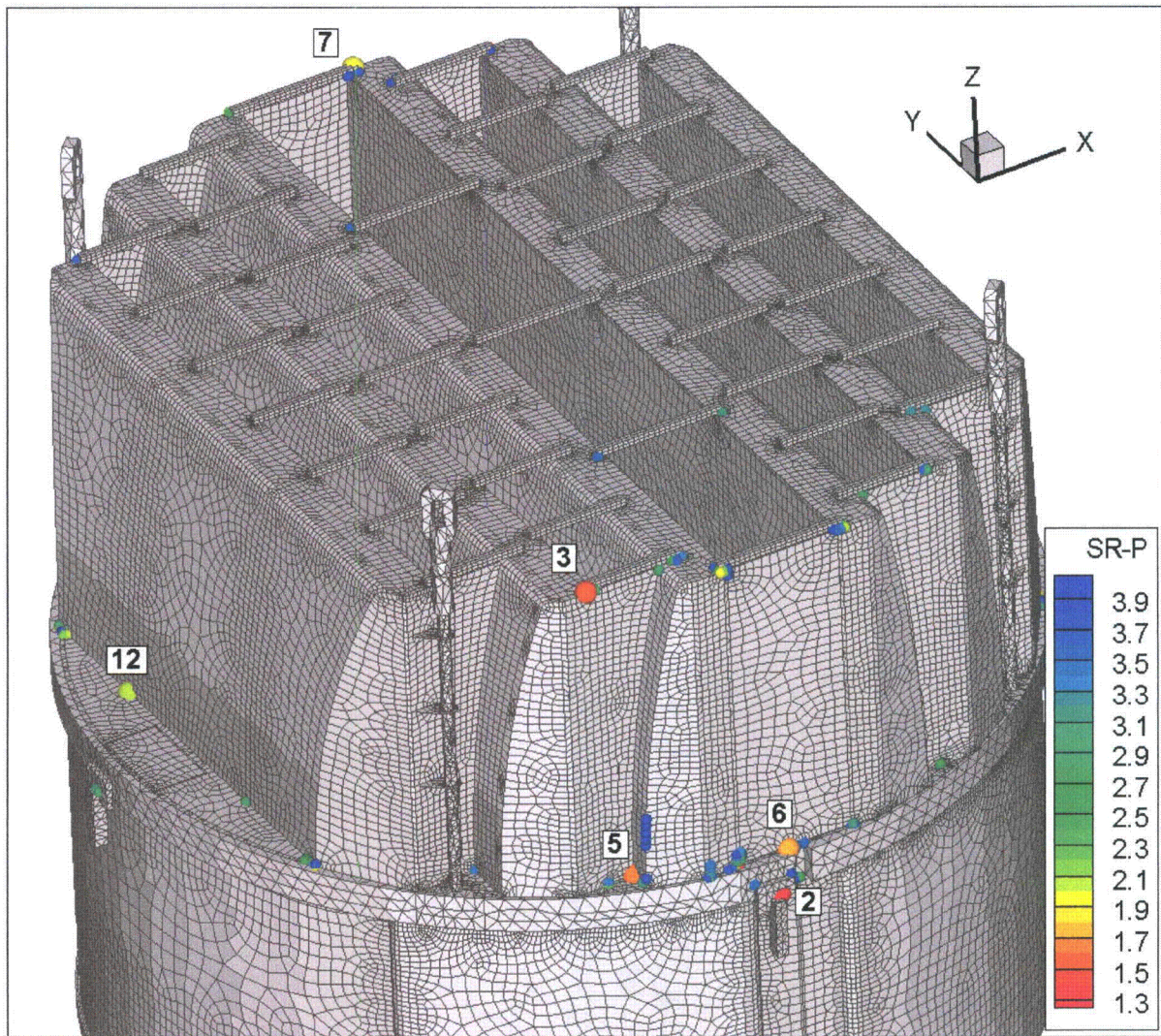


Figure 15d. Locations of minimum stress ratios,  $SR-P \leq 4$ , associated with maximum stresses at welds for CLTP operation with frequency shifts. The recorded stress ratio at a node is the minimum value taken over all frequency shifts. Numbers refer to the enumerated locations for SR-P values at welds in Table 9b. This view shows locations 2, 3, 5-7 and 12.

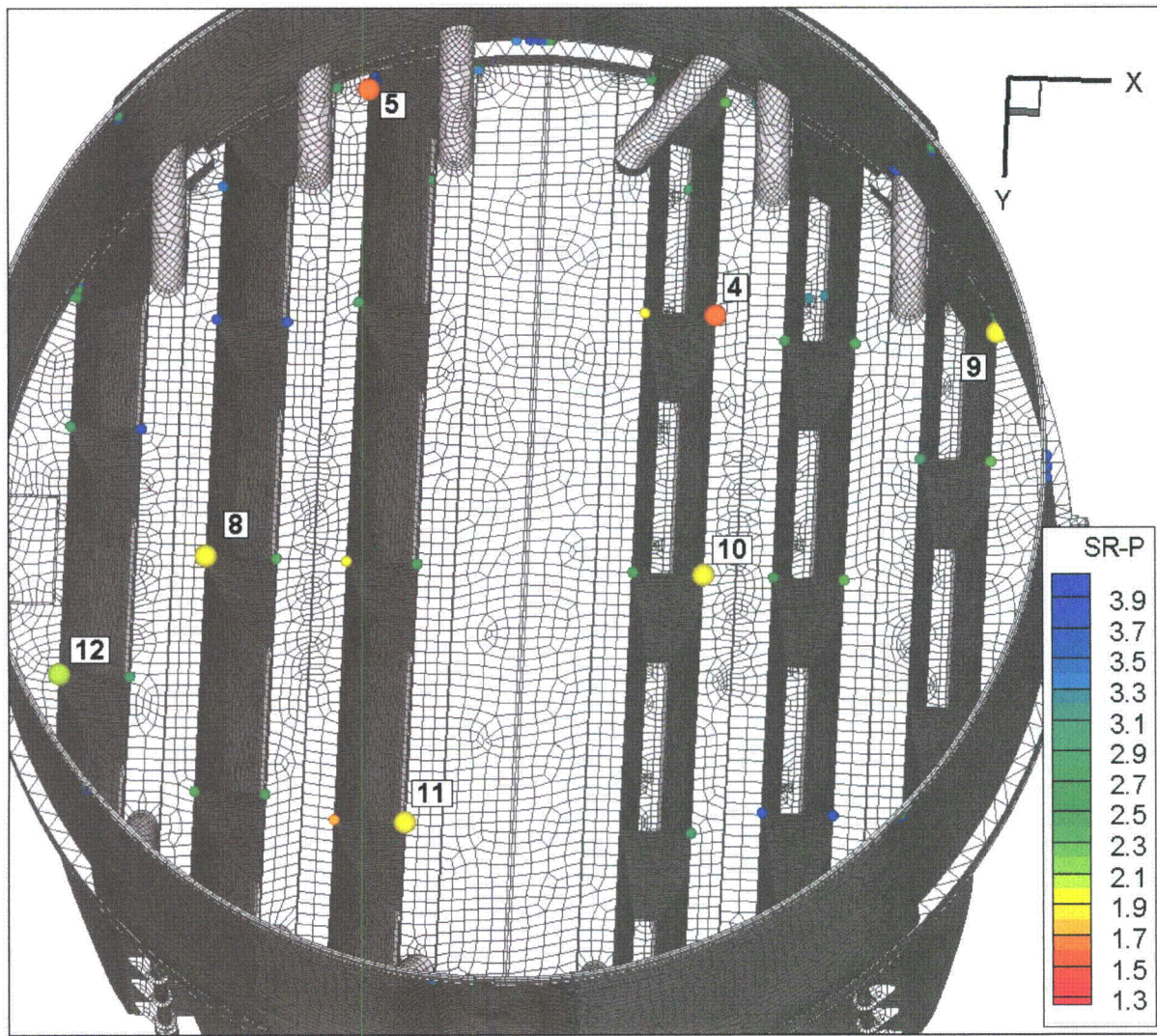


Figure 15e. Locations of minimum stress ratios,  $SR-P \leq 4$ , at welds for CLTP operation with frequency shifts. The recorded stress ratio at a node is the minimum value taken over all frequency shifts. Numbers refer to the enumerated locations for SR-P values at welds in Table 9b. This view from below shows locations 4, 5 and 8-12.

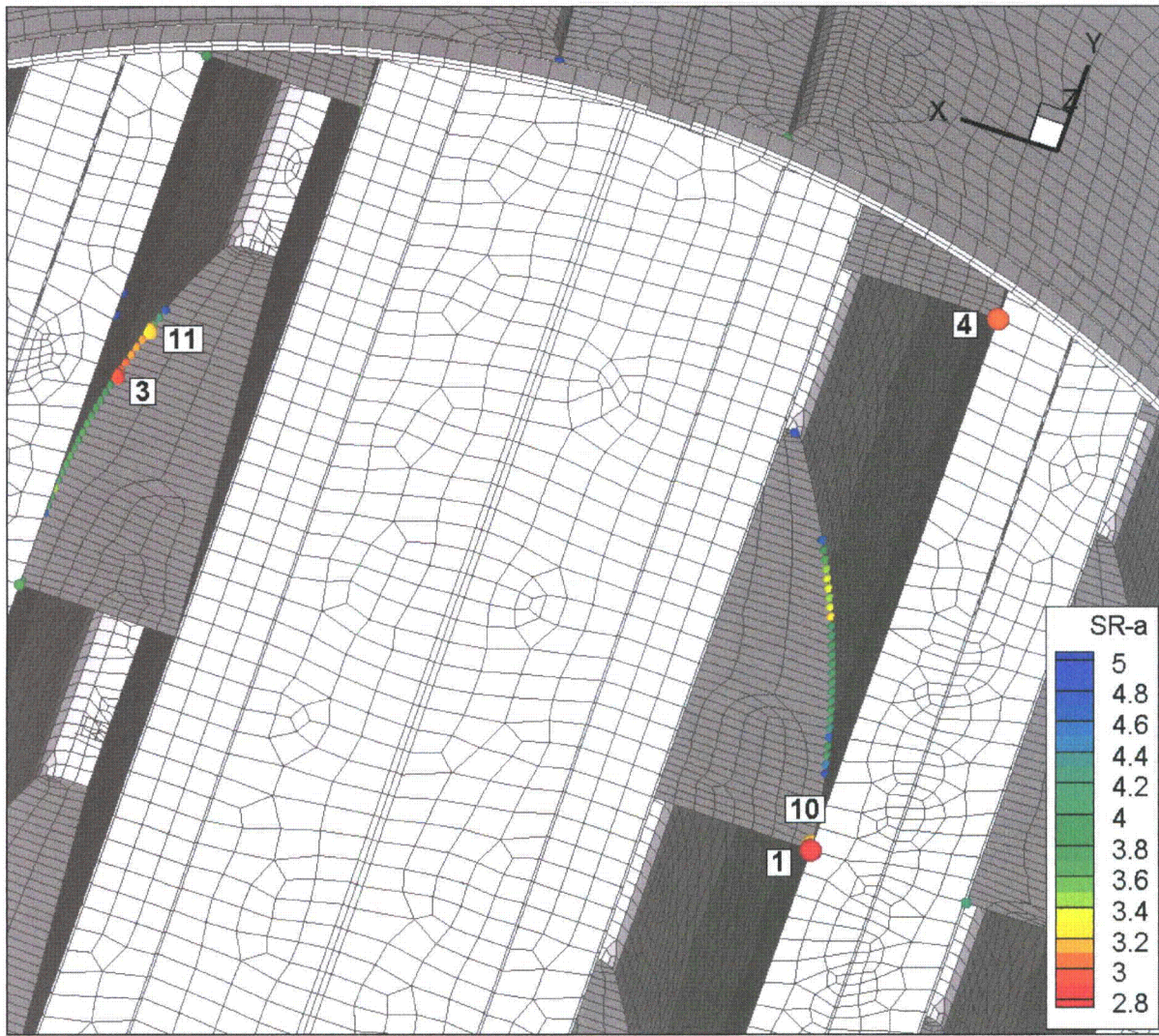


Figure 15f. Locations of minimum alternating stress ratios,  $SR-a \leq 5$ , at welds for CLTP operation with frequency shifts. The recorded stress ratio at a node is the minimum value taken over all frequency shifts. Numbers refer to the enumerated locations for SR-a values at welds in Table 9b. This view from below shows locations 1, 3, 4, 10 and 11 all on hood welds.

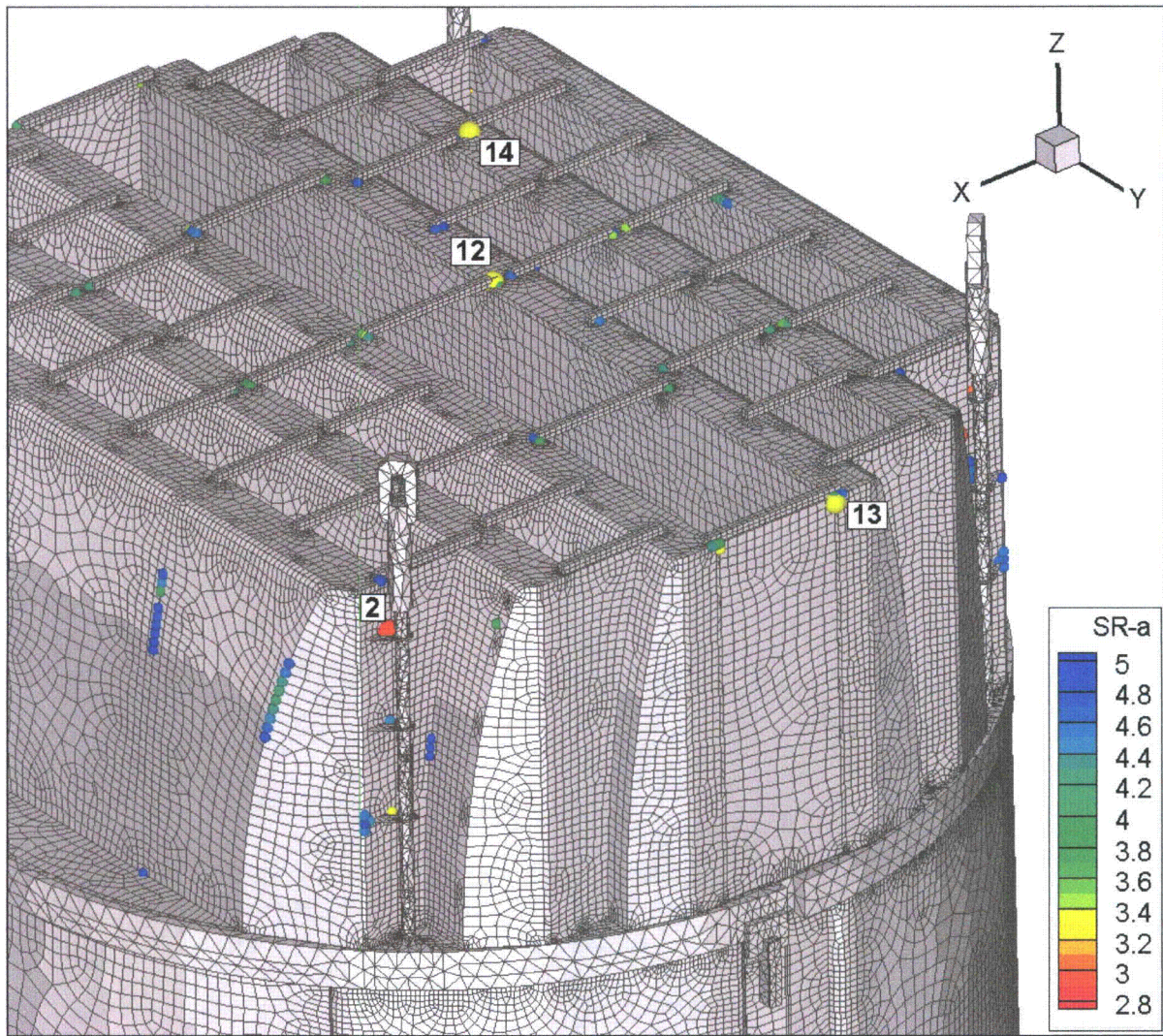


Figure 15g. Locations of minimum alternating stress ratios,  $SR-a \leq 5$ , at welds for CLTP operation with frequency shifts. The recorded stress ratio at a node is the minimum value taken over all frequency shifts. Numbers refer to the enumerated locations for  $SR-a$  values at welds in Table 9b. This view shows locations 2 and 12-14.

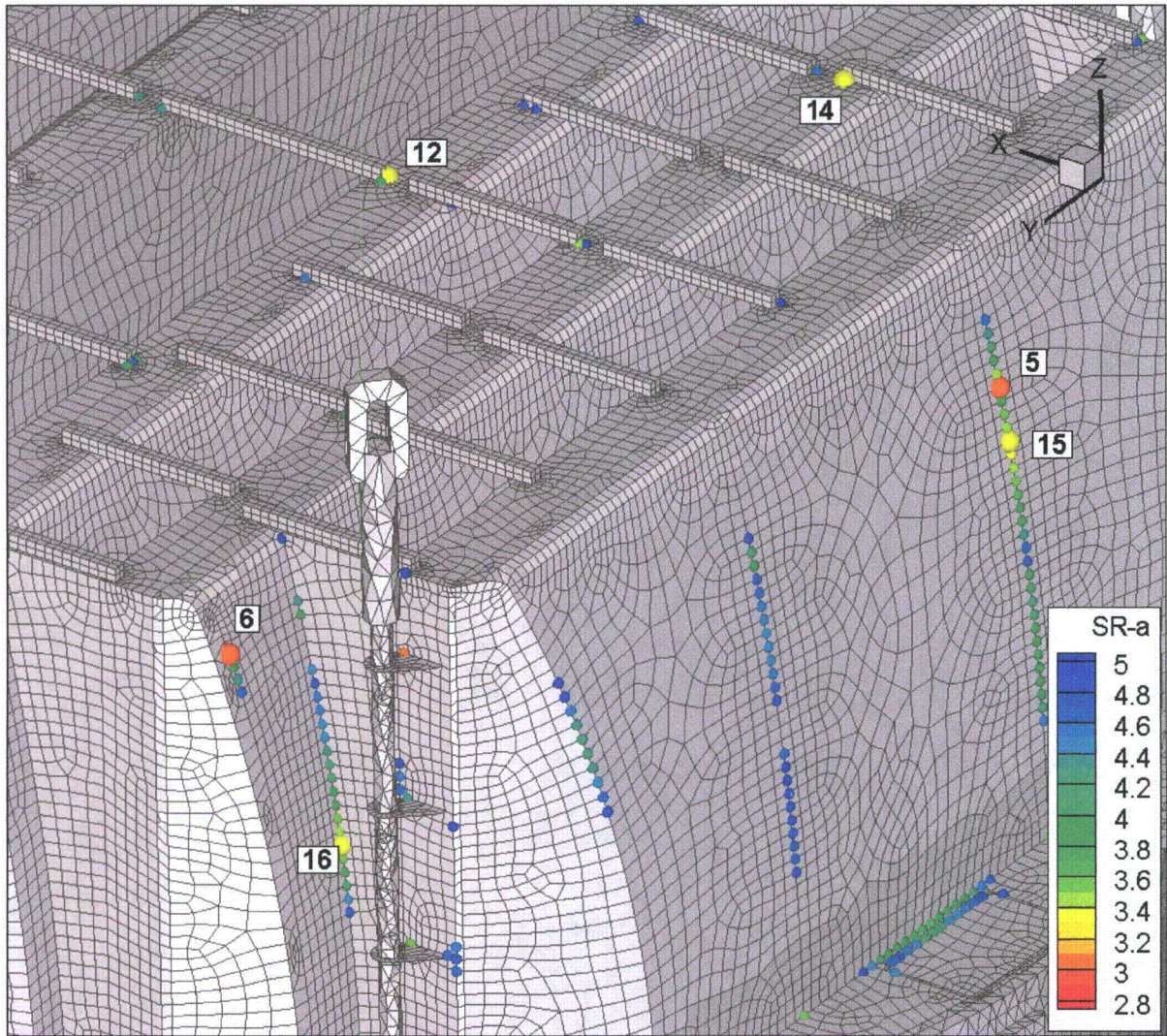


Figure 15h. Locations of minimum alternating stress ratios,  $SR-a \leq 5$ , at welds for CLTP operation with frequency shifts. The recorded stress ratio at a node is the minimum value taken over all frequency shifts. Numbers refer to the enumerated locations for SR-a values at welds in Table 9b. Close-up view showing locations 5, 6, 12 and 14-16.

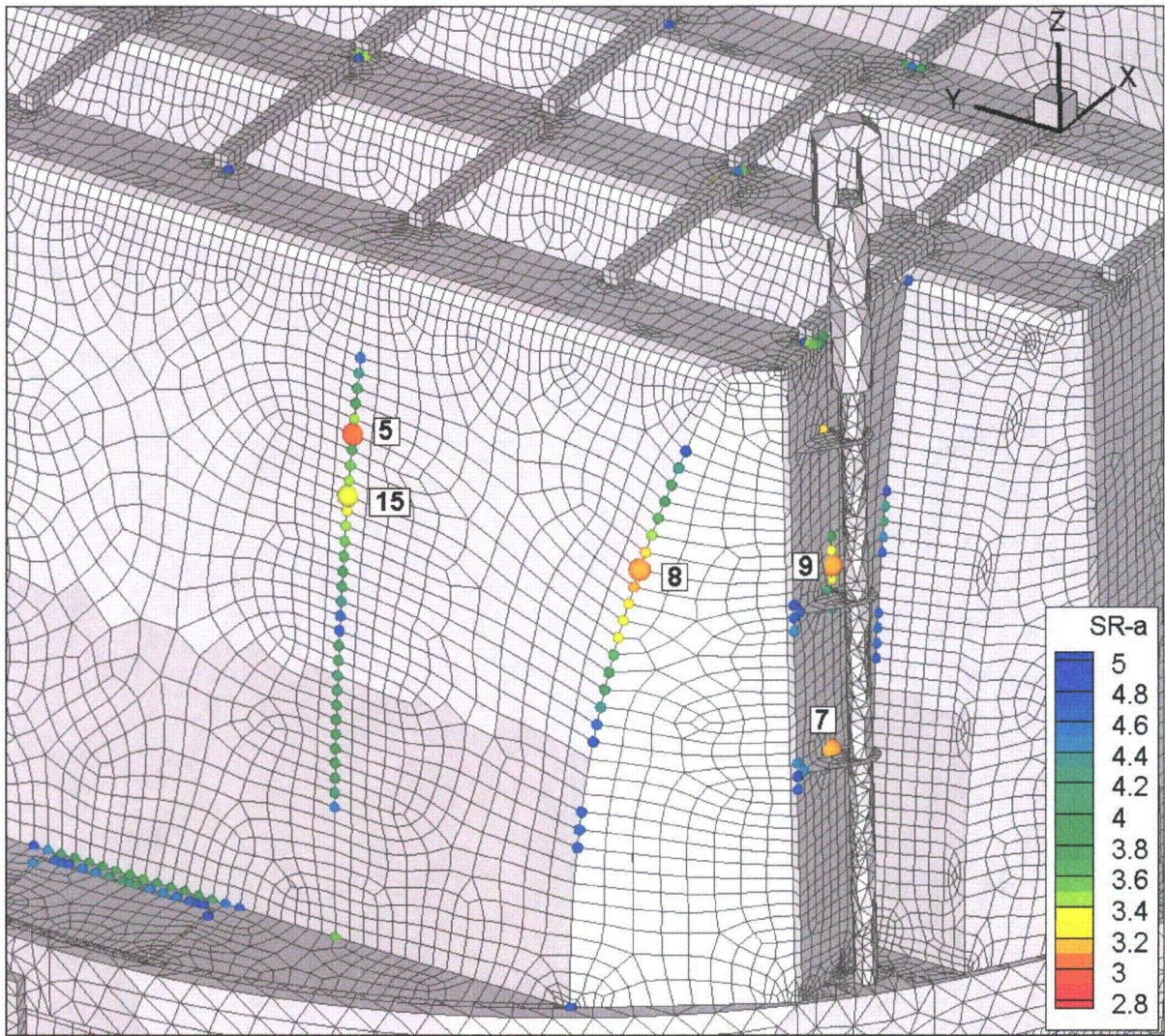


Figure 15i. Locations of minimum alternating stress ratios,  $SR-a \leq 5$ , at welds for CLTP operation with frequency shifts. The recorded stress ratio at a node is the minimum value taken over all frequency shifts. Numbers refer to the enumerated locations for  $SR-a$  values at welds in Table 9b. Close-up view around locations 5, 7-9 and 15.

### 5.3 Frequency Content and Filtering of the Stress Signals

The frequency contribution to the stresses can be investigated by examining the power spectral density (PSD) curves and accumulative PSDs for selected nodes having low alternating stress ratios. The accumulative PSDs are computed directly from the Fourier coefficients as

$$\Sigma(\omega_n) = \sqrt{\sum_{k=1}^n |\tilde{\sigma}(\omega_k)|^2}$$

where  $\tilde{\sigma}(\omega_k)$  is the complex stress harmonic at frequency,  $\omega_k$ . Accumulative PSD plots are useful for determining the frequency components and frequency ranges that make the largest contributions to the fluctuating stress. Unlike PSD plots, no “binning” or smoothing of frequency components is needed to obtain smooth curves. Steep step-like rises in  $\Sigma(\omega)$  indicate the presence of a strong component at a discrete frequency whereas gradual increases in the curve imply significant content over a broader frequency range. From Parseval’s theorem, equality between  $\Sigma(\omega_N)$  (where N is the total number of frequency components) and the RMS of the stress signal in the time domain is established.

The selected nodes are the ones having the lowest alternating stress ratios (at a weld) in Table 9b. These are:

- Node 85723 – located on the inner hood/hood support/middle base plate junction. The associated PSDs are shown in Figure 16a.
- Node 89649 - located on the lifting rod brace/vane bank end plate connection. The associated PSDs are shown in Figure 16b.
- Node 99529 – located on the weld joining the inner hood and hood support. The associated PSDs are shown in Figure 16c.
- Node 99212 – located on the weld joining the outer hood and its end plate. The associated PSDs are shown in Figure 16d.
- Node 87780 – located on the weld joining the closure plate to the outer closure plate to the outer vane bank. The associated PSDs are shown in Figure 16e.

These are the nodes labeled 1-3, 8 and 9 in Table 9b and accompanying Figure 15f-i.

In each case, since there are six stress components and up to three different section locations for shells (the top, mid and bottom surfaces), there is a total of 18 stress histories per component. Moreover, at junctions there are at least two components that meet at the junction. The particular stress component that is plotted is chosen as follows. First, the component and section location (top/mid/bottom) is taken as the one that has the highest alternating stress. This narrows the selection to six components. Of these, the component having the highest Root Mean Square (RMS) is selected.

The first node (85723), is dominated by a broad peak centered at 71 Hz. The frequency shifted curves do not differ significantly from the non-shifted results. Judging from the PSD curves, it appears that in the non-shifted case there are two peaks about 71 Hz, with one – the

lower frequency one - being dominant. When the signal is shifted, the forcing on the lower frequency mode is reduced and that on the higher frequency mode increases. Interestingly, the combined effect is to effectively shift the peak frequency upward even though the signal is shifted downward (as is clear by comparing some of the other peaks). This effect is readily explainable in the context of the complex multi-modal system being considered here. Frequency shifting has a more pronounced effect on node 89649 which has dominant frequencies at 13.4 Hz, 19.6 Hz and 136 Hz. The lower frequency peaks grow, but do not shift significantly with the +10% frequency shift. The higher frequency peak appears to shift and attenuate with the frequency shift in the signal. The third node is dominated by a 45.4 Hz peak. This dominance appears to be spatially localized meaning that the number of locations on the dryer where this is the dominant frequency, are few. However, the same frequency peak shows up in the limiting location at node 85723 which also involves the inner hood suggesting that the inner hood is responsive to acoustic signals at this frequency. The stress response at node 99212 is also characterized by a single dominant the dominant peak, this time at a frequency between 69 and 71 Hz. This frequency characterizes most of the surface on the outer panels of the outer hood on the MSL C/D side. Finally for node 87780, the dominant stress contributions occur at higher frequencies. Without frequency shifting the dominant frequency is 180.0 Hz which coincides with a multiple of electrical noise (60 Hz - note however, that the electrical noise is filtered). At the +7.5% shift the dominant frequency is at 184.5 Hz which corresponds to 171.6 Hz in the original non-shifted signal.

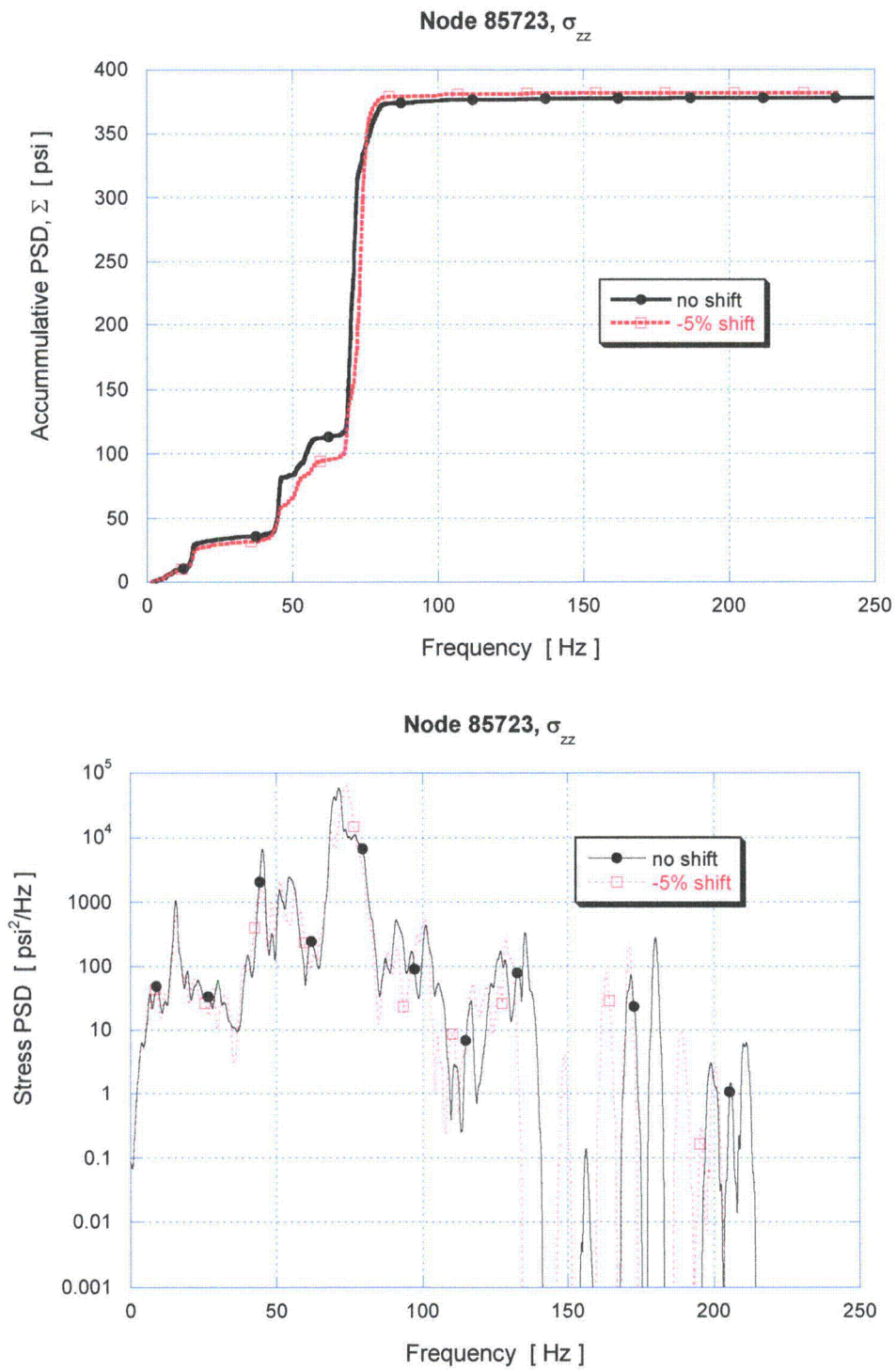


Figure 16a. Accumulative PSD and PSD curves of the  $\sigma_{zz}$  stress response at node 85723.

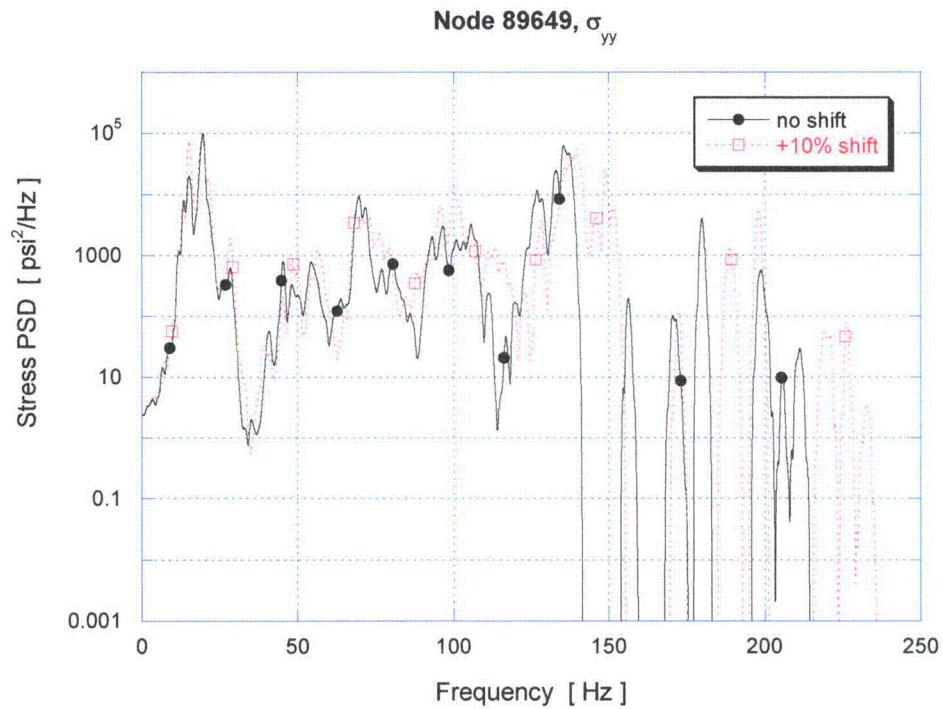
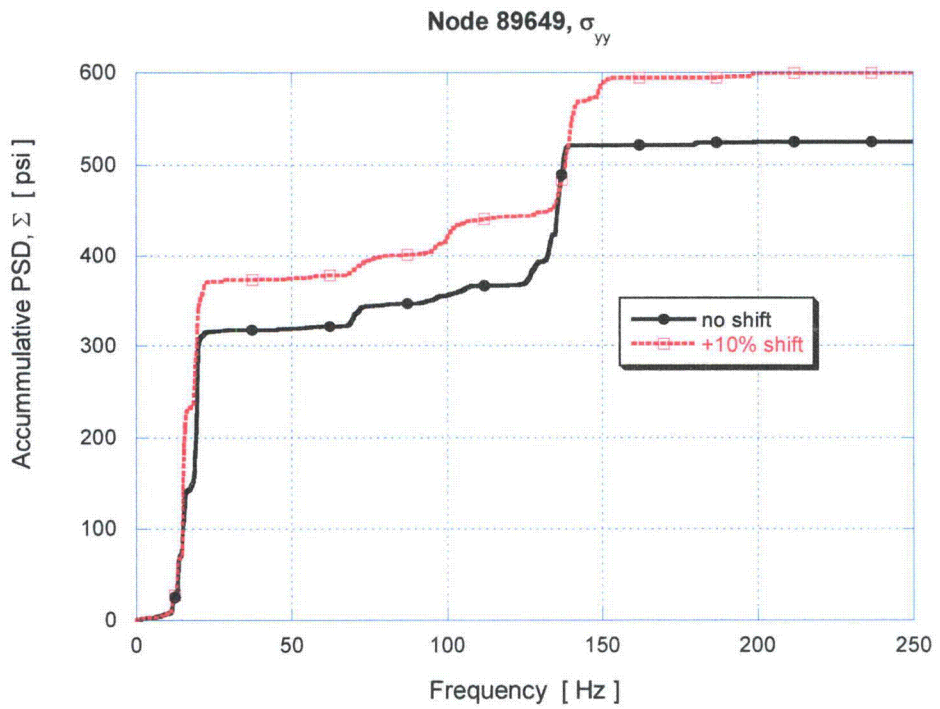


Figure 16b. Accumulative PSD and PSD of the  $\sigma_{yy}$  stress response at node 89649.

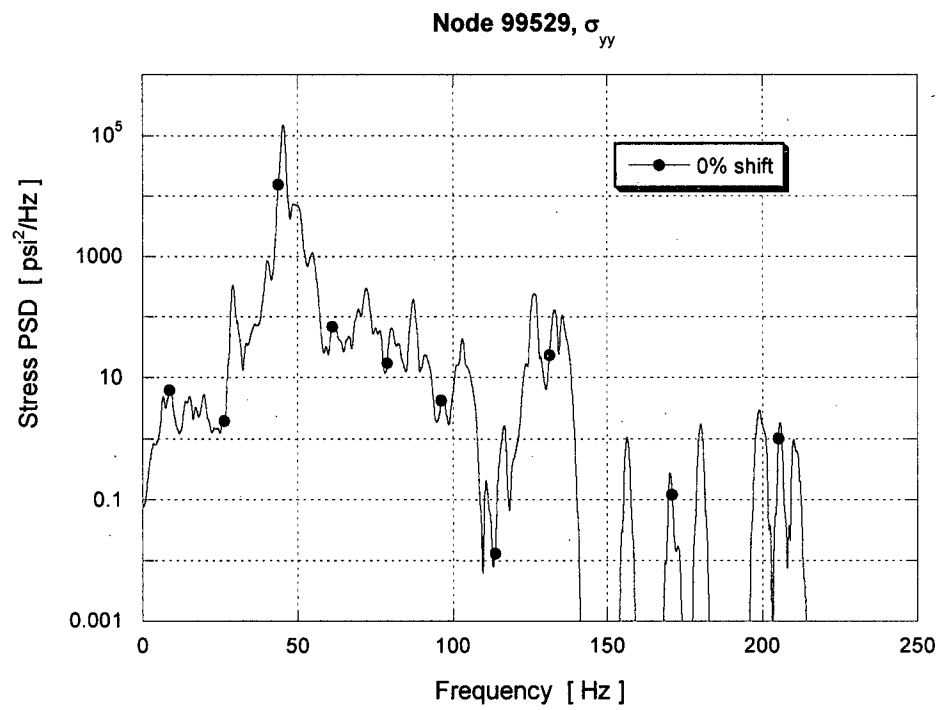
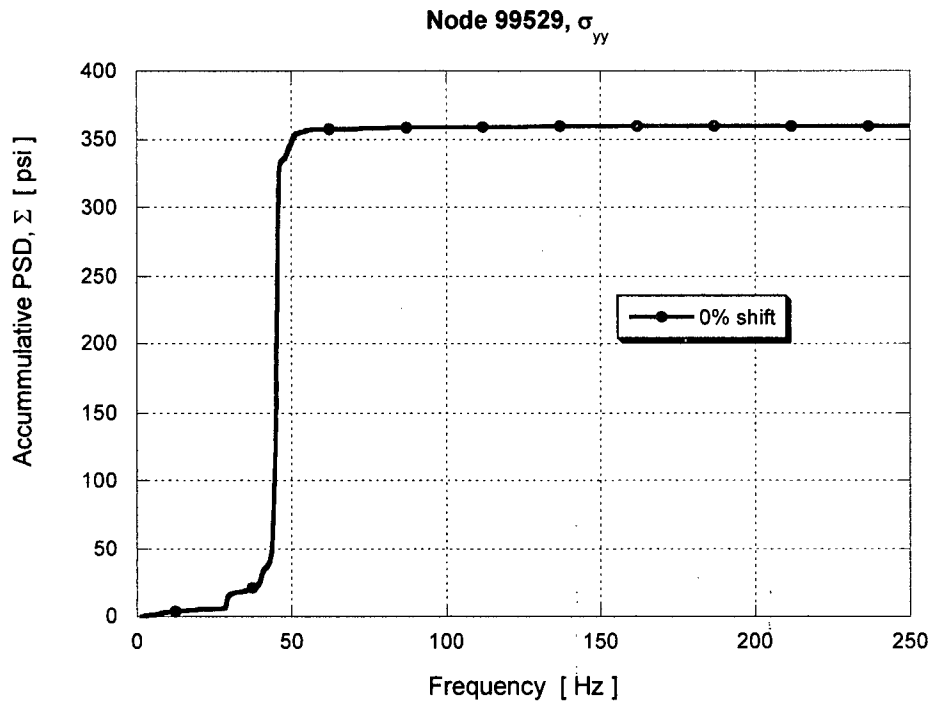


Figure 16c. Accumulative PSD and PSD of the  $\sigma_{yy}$  stress response at node 99529.

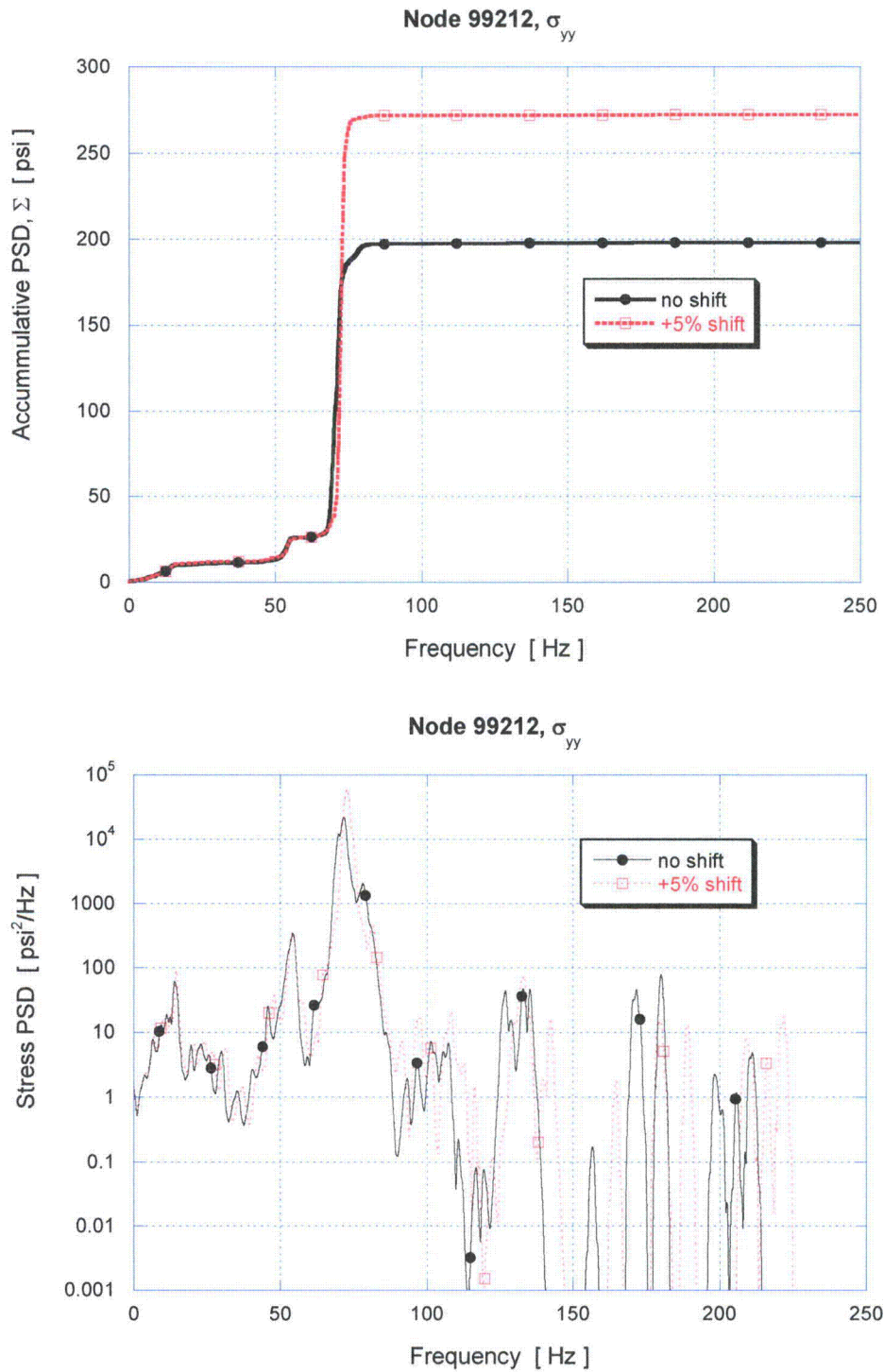


Figure 16d. Accumulative PSD and PSD of the  $\sigma_{yy}$  stress response at node 99212.

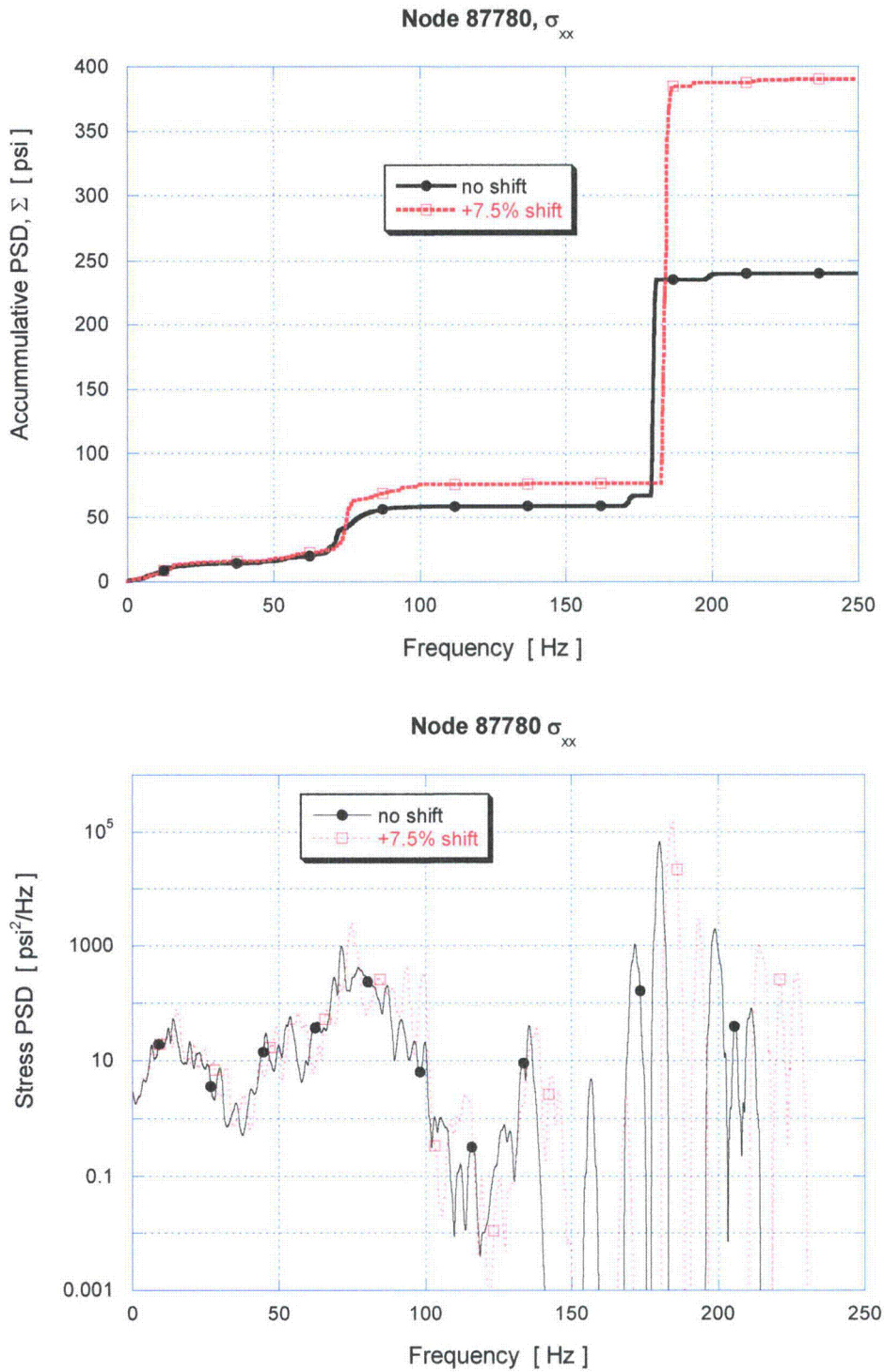


Figure 16e. Accumulative PSD and PSD of the  $\sigma_{xx}$  stress response at node 87780.

## 6. Conclusions

A frequency-based steam dryer stress analysis has been used to calculate high stress locations and calculated / allowable stress ratios for the Nine Mile Point Unit 2 steam dryer at CLTP load conditions using plant measurement data. A detailed description of the frequency-based methodology and the finite element model for the NMP Unit 2 steam dryer is presented. The CLTP loads obtained in a separate acoustic circuit model [3] including end-to-end bias and uncertainty for both the ACM [3] and FEA were applied to a finite element model of the steam dryer consisting mainly of the ANSYS Shell 63 elements, brick continuum elements and beam elements.

The measured CLTP loads are applied without filtering of low power data. The resulting stress histories were analyzed to obtain maximum and alternating stresses at all nodes for comparison against allowable levels. These results are tabulated in Table 9 of this report. The minimum alternating stress ratio at nominal operation is  $SR-a=3.00$  and the minimum alternating stress ratio taken over all frequency shifts is  $SR-a=2.89$ . The stress ratio associated with maximum stress intensities varies weakly with frequency shift and assumes a minimum value of  $SR-P=1.34$  both with and without frequency shifting.

Since flow-induced acoustic resonances are not anticipated in the steam dryer, the alternating stress ratios at EPU operation can be obtained by scaling the CLTP values by the steam flow velocity squared,. Under this approach, the limiting alternating stress ratio becomes  $SR-a=2.89/1.388=2.08$ . For the node with the limiting maximum stress ratios at CLTP, the corresponding limiting value at EPU is  $SR-P=1.32$ . Given that the alternating stress ratio  $SR-a$  obtained at EPU remains above 2.08 at all frequency shifts together with the comparatively small dependence of  $SR-P$  upon acoustic loads, the Unit 2 dryer is expected to qualify at EPU conditions.

Frequency Shift	Minimum Stress Ratio at CLTP		Min. Alt. Stress Ratio (SR-a) at EPU
	Max. Stress, SR-P	Alternating Stress, SR-a	
0% (nominal)	1.34	3.00	2.16
-10%	1.36	3.09	2.23
-7.5%	1.36	3.07	2.21
-5%	1.36	2.89	2.08
-2.5%	1.36	3.27	2.36
+2.5%	1.36	2.93	2.11
+5%	1.34	2.97	2.14
+7.5%	1.35	3.07	2.21
+10%	1.35	2.93	2.11
All shifts	1.34 – 1.36	2.89 – 3.27	2.08 – 2.36
<b>Limiting</b>	<b>1.34</b>	<b>2.89</b>	<b>2.08</b>

## 7. References

1. ASME Boiler and Pressure Vessel Code, Section III, Subsection NG (2007).
2. Continuum Dynamics, Inc. (2005), *Methodology to Determine Unsteady Pressure Loading on Components in Reactor Steam Domes* (Rev. 6), C.D.I. Report No. 04-09 (Proprietary).
3. Continuum Dynamics, Inc. (2008), *Acoustic and Low Frequency Hydrodynamic Loads at CLTP Power Level on Nine Mile Point Unit 2 Steam Dryer to 250 Hz, Rev. 2*, C.D.I. Report No. 08-08P (Proprietary).
4. Continuum Dynamics, Inc. (2007), *Methodology to Predict Full Scale Steam Dryer Loads from In-Plant Measurements, with the Inclusion of a Low Frequency Hydrodynamic Contribution*, C.D.I. Report No. 07-09P (Proprietary).
5. Structural Integrity Associates, Inc. (2009), *Nine Mile Point Unit 2 Steam Dryer Closure Plates Analysis Results*, SIA Letter Report No. 0900895.401 Revision 0, August 21.
6. Structural Integrity Associates, Inc. (2008), *Nine Mile Point Unit 2 Main Steam Line Strain Gage Data Reduction*, SIA Calculation Package No. NMP-26Q-302.
7. Continuum Dynamics, Inc. (2007), *Response to NRC Request for Additional Information on the Hope Creek Generating Station, Extended Power Uprate*, RAI No. 14.110.
8. Structural Integrity Associates, Inc. (2008), *Flaw Evaluation and Vibration Assessment of the Nine Mile Point Unit 2 Steam Dryer for Extended Power Uprate Operating Conditions*, Report No. 0801273.401.
9. Continuum Dynamics, Inc. (2008), *Stress Assessment of Browns Ferry Nuclear Unit 1 Steam Dryer, Rev. 0*, C.D.I. Report No. 08-06P (Proprietary).
10. O'Donnell, W.J., *Effective Elastic Constants For the Bending of Thin Perforated Plates With Triangular and Square Penetration Patterns*. ASME Journal of Engineering for Industry, 1973. **95**: p. 121-128.
11. U.S. Nuclear Regulatory Commission (2007), *Comprehensive Vibration Assessment Program for Reactor Internals During Preoperational and Initial Startup Testing*, Regulatory Guide 1.20, March.
12. Weld Research Council (1998), *Fatigue Strength Reduction and Stress Concentration Factors For Welds In Pressure Vessels and Piping*, WRC Bulletin 432.
13. Pilkey, W.D., *Peterson's Stress Concentration Factors, 2nd ed.* 1997, New York: John Wiley. pg. 139.
14. Lawrence, F.V., N.-J. Ho, and P.K. Mazumdar, *Predicting the Fatigue Resistance of Welds*. Ann. Rev. Mater. Sci., 1981. **11**: p. 401-425.
15. General Electric (GE) Nuclear Energy, *Supplement 1 to Service Information Letter (SIL) 644, "BWR/3 Steam Dryer Failure," September 5, 2003*.
16. Tecplot, Inc. (2004), URL: <http://www.tecplot.com>, *Documentation: Tecplot User's Manual Version 10 Tecplot, Inc.*, October.
17. GE Nuclear Energy (2006), *Browns Ferry Nuclear Plant Units 1, 2, and 3 Steam Dryer Stress, Dynamic, and Fatigue Analysis for EPU Conditions*, GE-NE-0000-0053-7413-R4-NP.
18. Structural Integrity Associates, Inc. (2008), *Shell and Solid Sub-Model Finite Element Stress Comparison, Rev. 2*, Calculation Package, 0006982.301, Oct. 17.
19. Continuum Dynamics, Inc. (2008), *Stress Assessment of Browns Ferry Nuclear Unit 2 Steam Dryer with Outer Hood and Tie-Bar Reinforcements, Rev. 0*, C.D.I. Report No. 08-20P (Proprietary).
20. Structural Integrity Associates, Inc. (2008), *Comparison Study of Substructure and Submodel Analysis using ANSYS*, Calculation Package, 0006982.304, December.

This Document Does Not Contain Continuum Dynamics, Inc. Proprietary Information

21. Continuum Dynamics, Inc. (2009), *Response to NRC Round 23 RAI EMCB 201/162 part c*, January.
22. Continuum Dynamics, Inc. (2009), *Compendium of Nine Mile Point Unit 2 Steam Dryer Sub-Models Away From Closure Plates* C.D.I. Technical Note No. 09-16P (Proprietary), August.
23. Continuum Dynamics, Inc. (2008), *Response to NRC RAI EMCB 172*, June.

Appendix A Sub-modeling and Modification of Closure Plates

[[

<sup>(3)</sup>]]

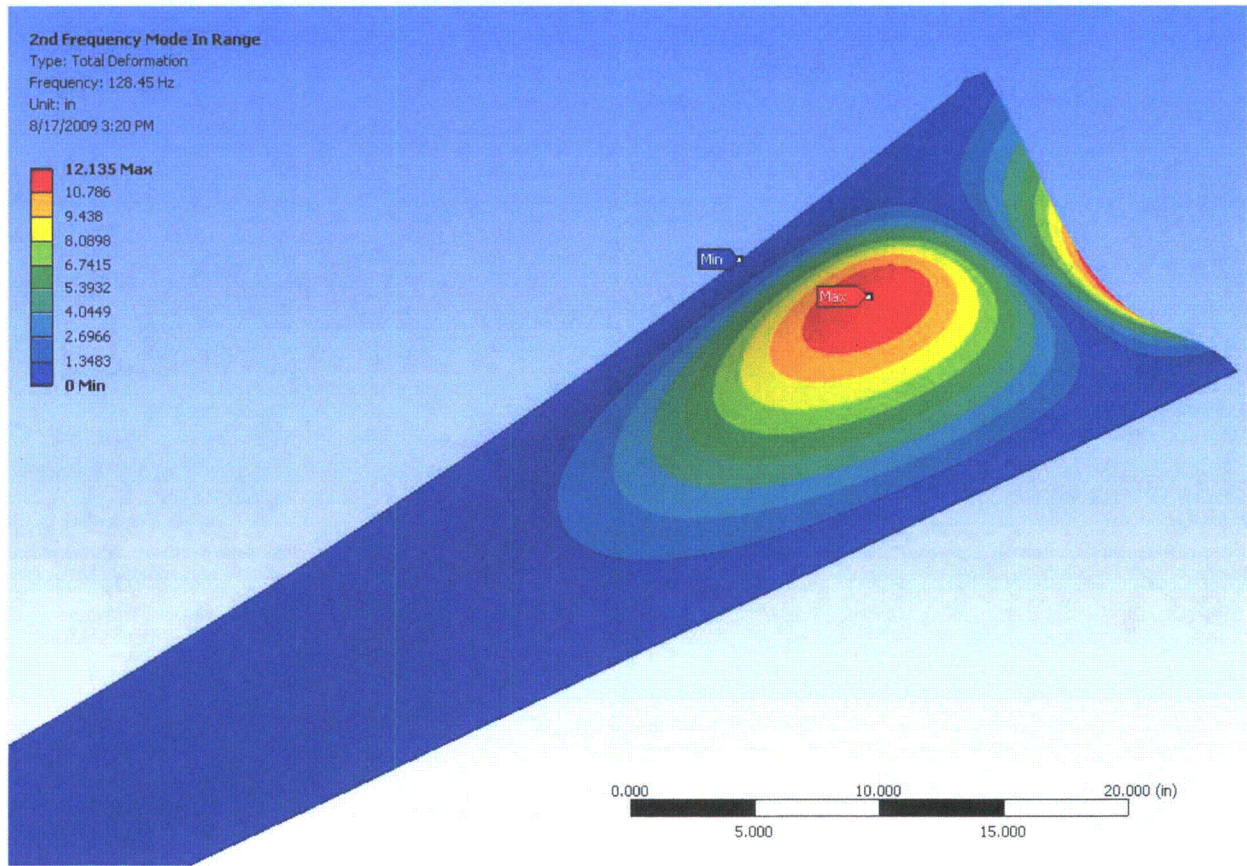


Figure 17: Second mode shape ( $f=128.45$  Hz) of unmodified closure plates

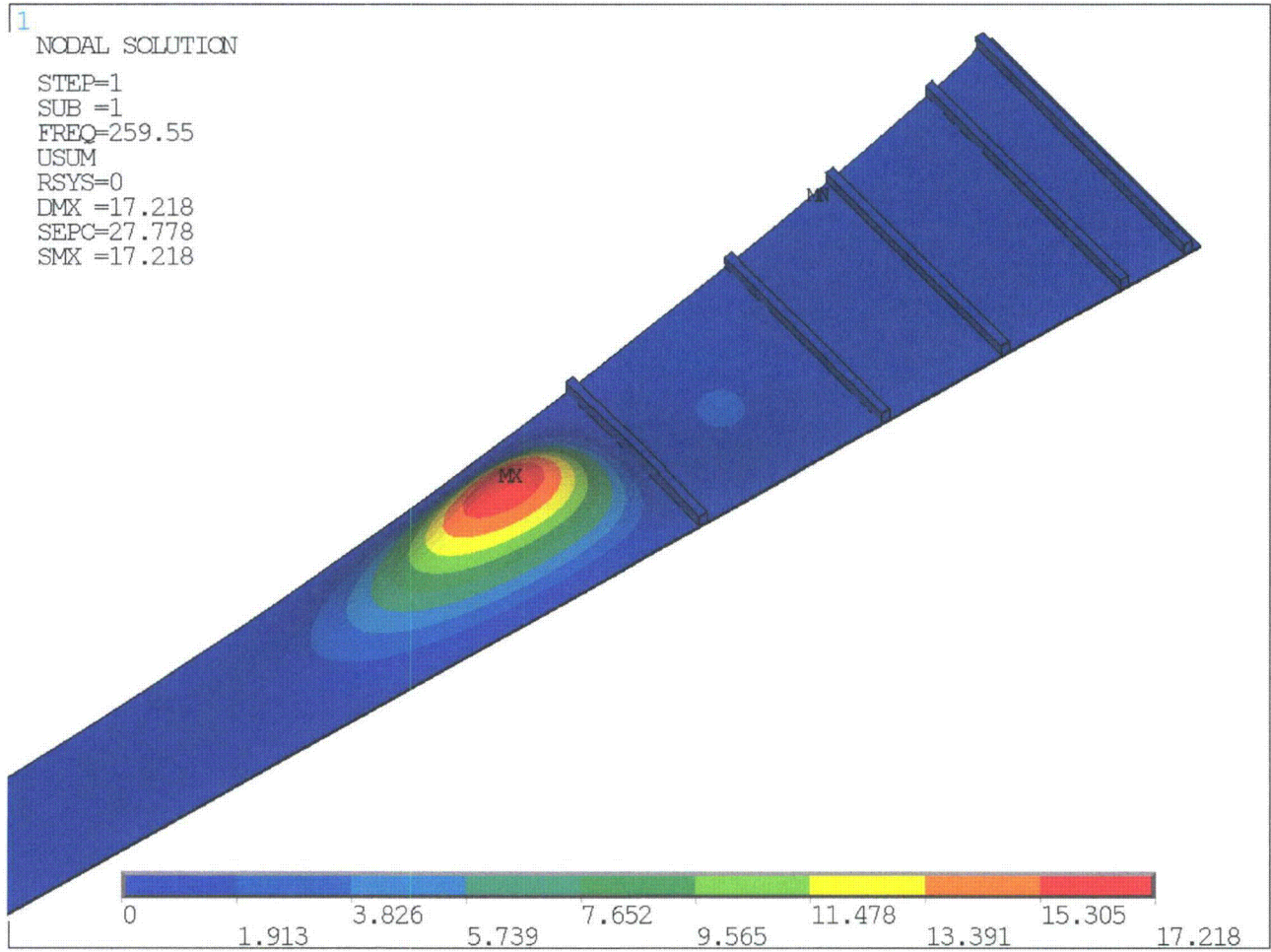


Figure 18: Fundamental mode shape ( $f=259.6$  Hz) of modified closure plate.

[[

<sup>(3)</sup>]]

[[

(3)]]

The sub-modeled locations together with the calculated stress reduction factors are given in Table 10. For each location depictions of the shell and solid element-based sub-models are given together with the applied loads/moments and resulting stresses. This is followed by a summary of the linearization paths and the limiting linearized stresses. The calculation of the stress reduction factor concludes the presentation for each location.

Table 10. List of sub-model locations

Location	x	y	z	node	Stress reduction factor
Top Thick Plate/Side Plate/Closure Plate/Top Plate	47.1	-108.6	88	101175	0.62
Closure Plate/Middle Hood	-63.8	85.2	72.5	91605	0.71
Closure Plate/Inner Hood	28.8	-108.6	87	95172	0.86
Side Plate/Closure Plate/Exit Top Perf/Exit Mid Top Perf	-47.1	108.6	74.5	100327	0.88

Note: The side plate/closure plate connection involving nodes 101175 and 100327 is reinforced on the interior side with a 0.25" weld. The hood/closure plate weld involving nodes 91605 and 95172 is reinforced on the interior side with a 0.125" weld.

### Sub model Node 101175

The sub-model for this node located at the top of the vertical weld joining the closure plate to the vane bank is shown in Figure 19a and involves five different components. The extracted forces are shown in Figure 19b. The shell sub-model stress distribution is shown in Figure 19c with a maximum (i.e., the maximum taken over all components and surfaces – top, bottom and middle) stress intensity stress at the location of 3362 psi. The corresponding solid sub-model together with mesh details and the stress distribution resulting when the same loads used in the shell sub-model are applied, are shown in Figure 20. Finally, the stress intensity linearization paths and corresponding linearized stresses extracted from the solid model are shown in Figure 21 and tabulated in Table 11. The limiting linearized stress in the solid sub-model is **2088 psi**. Comparing this value against the one obtained in the shell sub-model (**3362 psi**) yields the stress reduction factor:  $2088/3362 = 0.62$ .

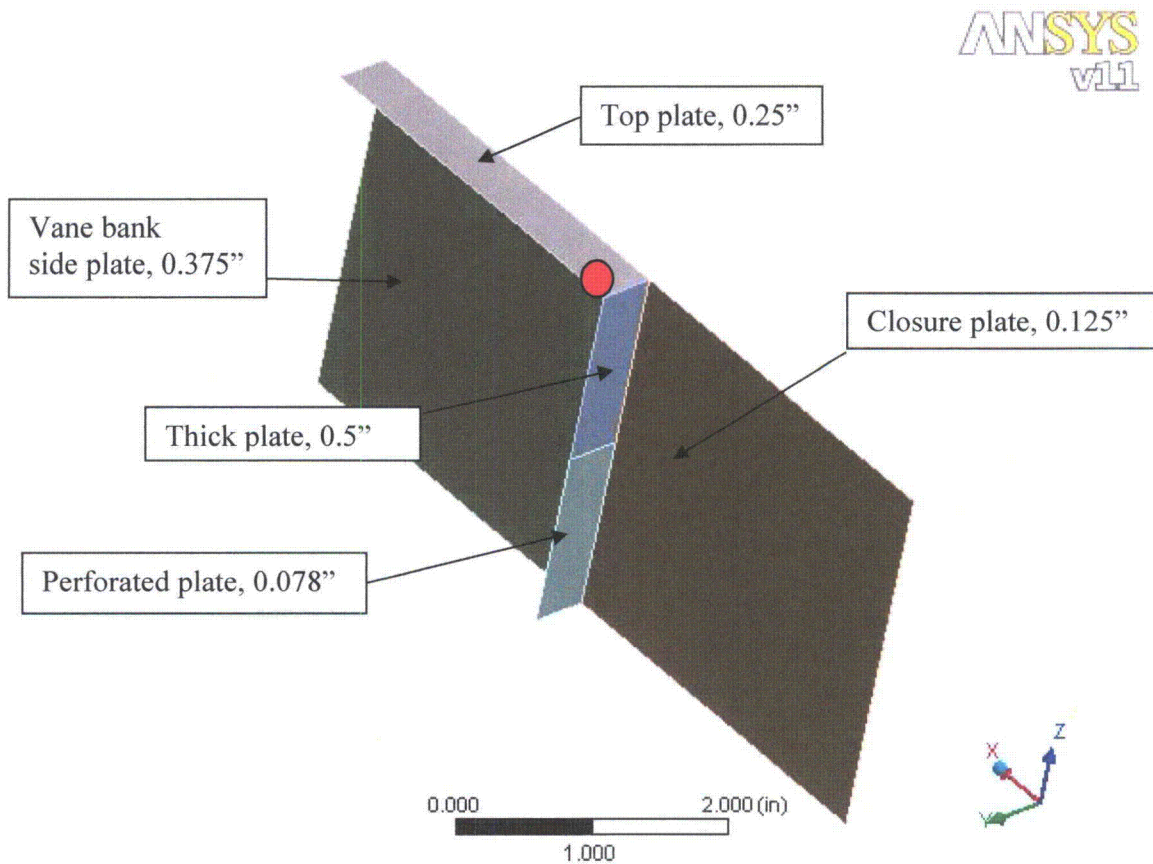


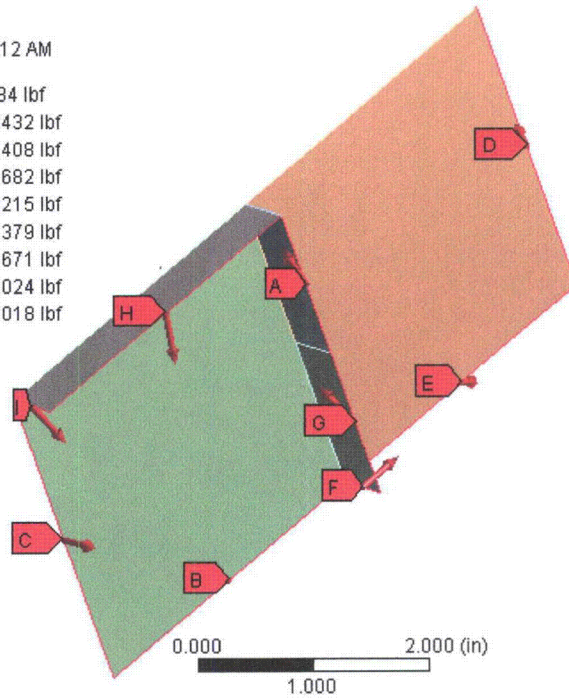
Figure 19a. Shell sub-model node 101175.



**Force 9**

Time: 1. s  
12/10/2008 10:12 AM

- A** Force: 14.684 lbf
- B** Force 2: 2.5432 lbf
- C** Force 3: 60.408 lbf
- D** Force 4: 29.682 lbf
- E** Force 5: 6.6215 lbf
- F** Force 6: 25.379 lbf
- G** Force 7: 2.0671 lbf
- H** Force 8: 41.024 lbf
- I** Force 9: 5.7018 lbf



**Moment 9**

Time: 1. s  
12/10/2008 10:13 AM

- A** Moment: 6.5096 lbf·in
- B** Moment 2: 8.1909 lbf·in
- C** Moment 3: 5.6901 lbf·in
- D** Moment 4: 6.7147 lbf·in
- E** Moment 5: 3.8973 lbf·in
- F** Moment 6: 6.1644e-003 lbf·in
- G** Moment 7: 8.9112e-002 lbf·in
- H** Moment 8: 2.4226 lbf·in
- I** Moment 9: 0.14082 lbf·in

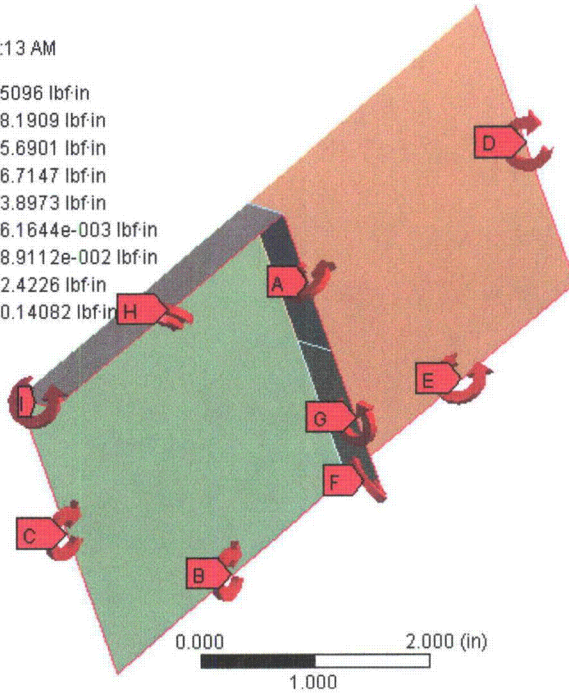


Figure 19b. Forces and moments.

**Stress Intensity**

Type: Stress Intensity - Top/Bottom

Unit: psi

Time: 1

12/10/2008 10:39 AM

**ANSYS**  
v11

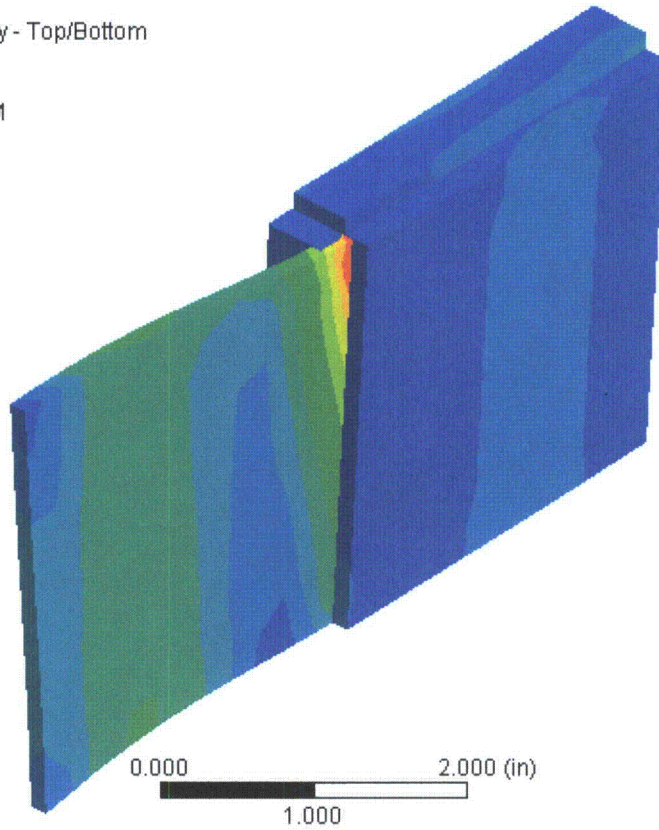
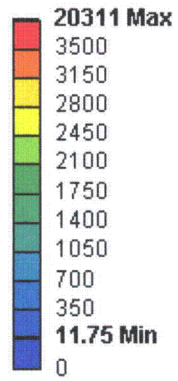


Figure 19c. Shell sub-model stress contours. Stress intensity: 3362 psi.

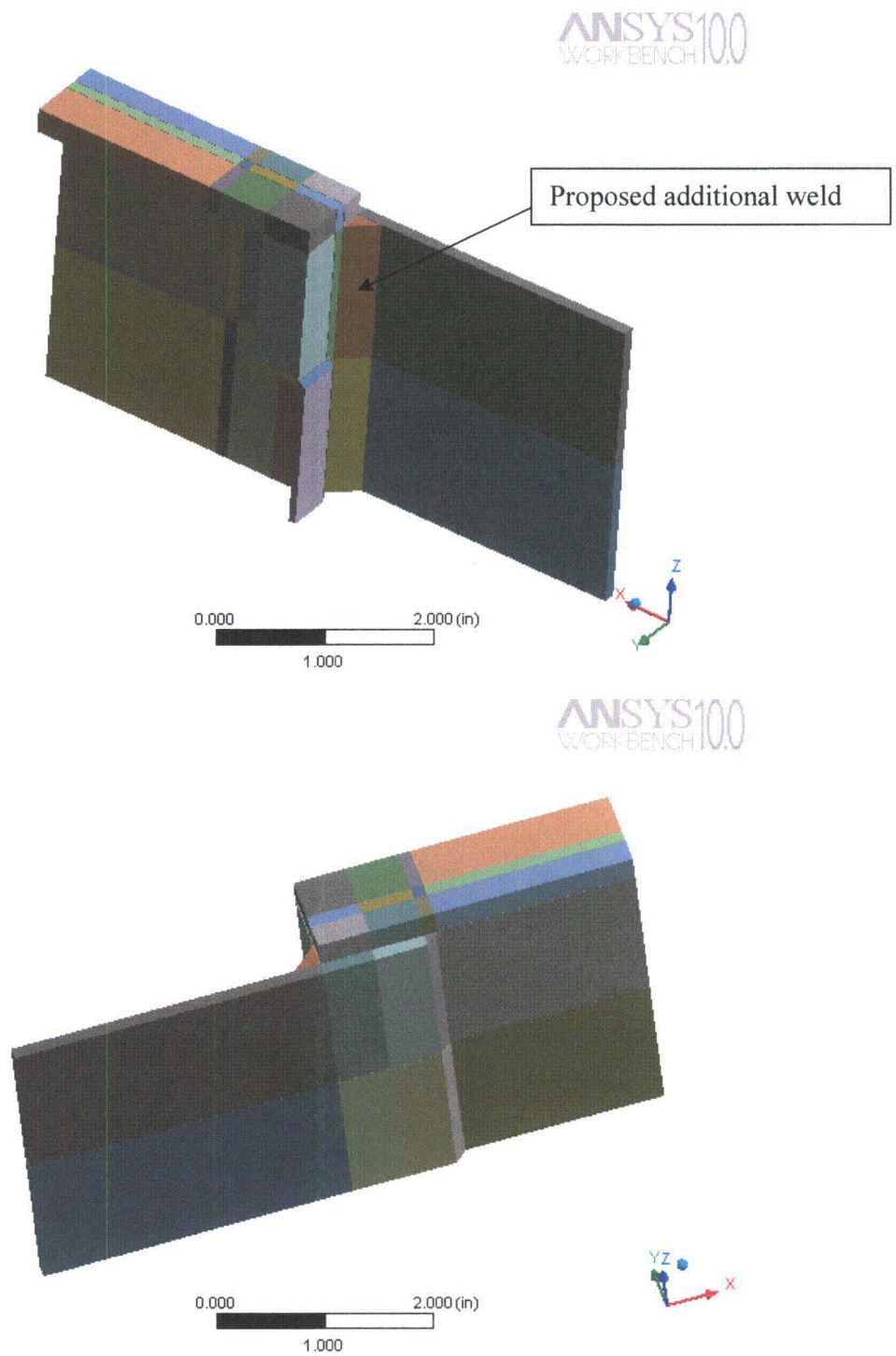


Figure 20a. Solid model geometry.

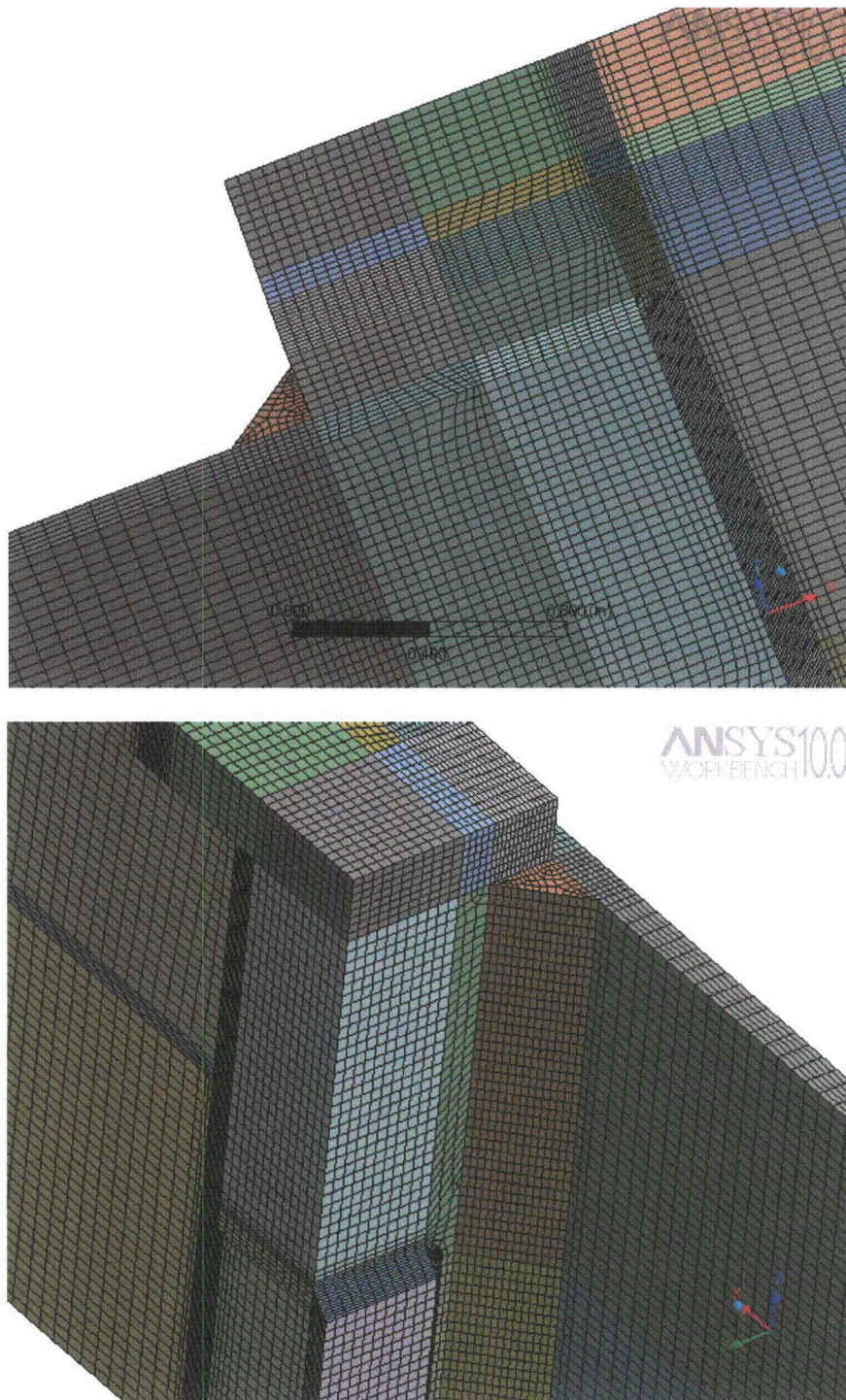


Figure 20b. Mesh overview. Mesh parameters: 748,327 nodes, 176,028 elements.

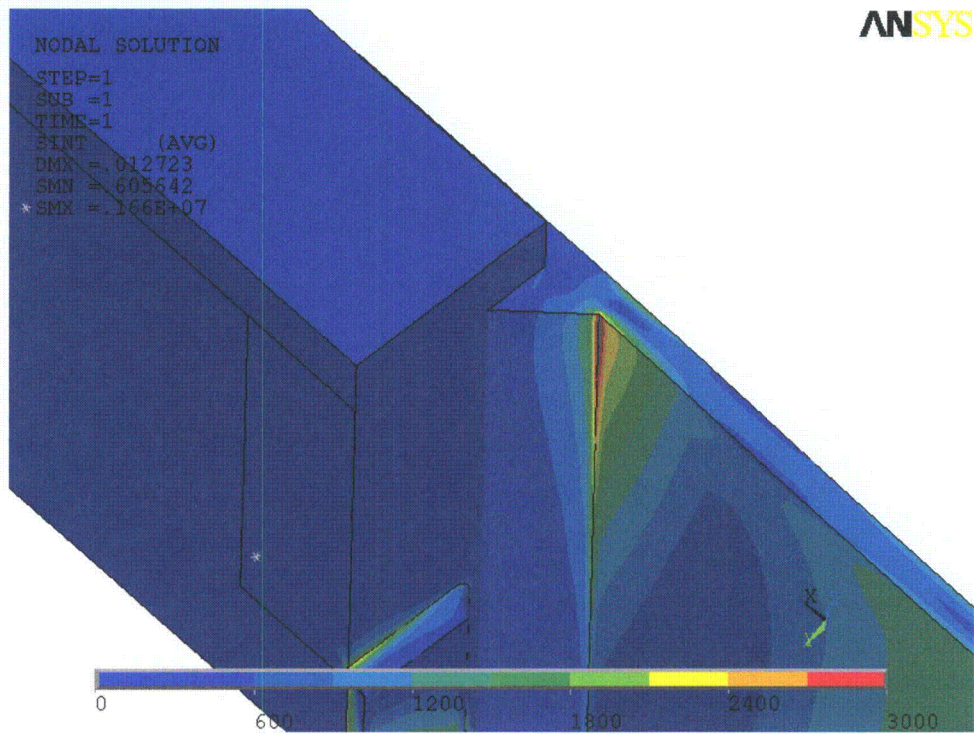
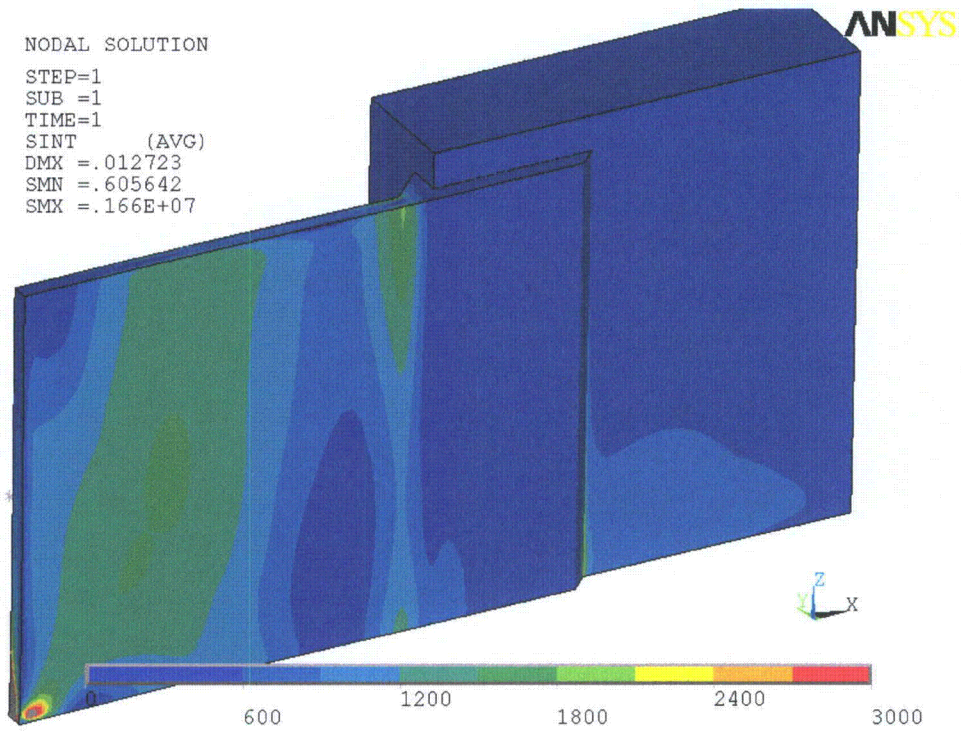


Figure 20c. Stress intensity contours (total) in solid sub-model.

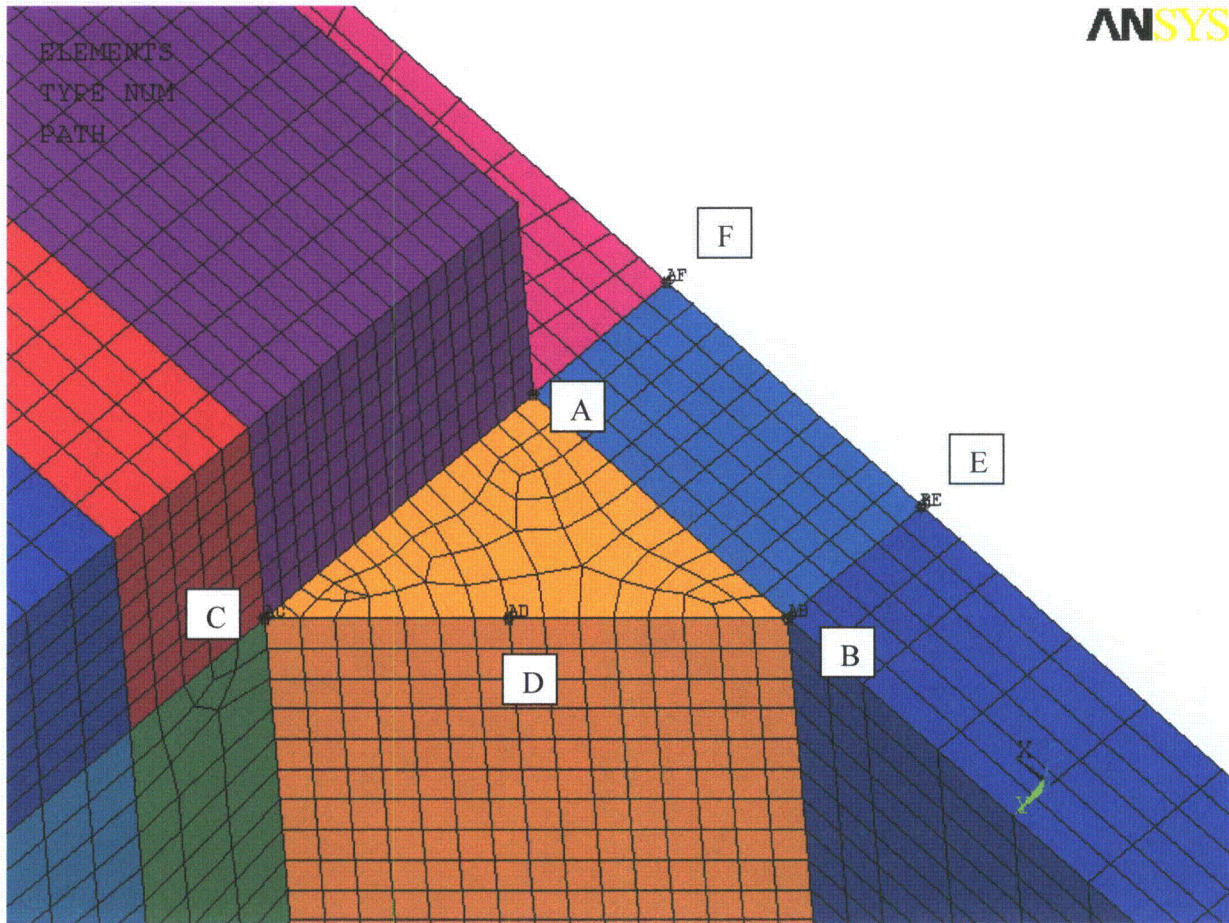


Figure 21. Linearization paths for sub-model node 101175.

Table 11. Linearized stresses along the linearization paths shown in Figure 21.

Path	Membrane + bending linearized stress intensity, psi
AB	1605
AC	710
AD	689
AF	492
BE	2088

**Sub model node 91605.**

The sub-model for this node located on the weld connecting the closure plate to the hood is shown in Figure 22a and involves two different components - the hood and closure plate. The extracted forces are shown in Figure 22b. The shell sub-model stress distribution is shown in Figure 22c with a maximum (i.e., the maximum taken over all components and surfaces – top, bottom and middle) stress intensity stress at the location of 3176 psi. The stresses in the corners are neither singularities nor due to constraint forces (they arise regardless of where the model is supported). When the sub-model mesh is refined these stresses do not grow. Instead they essentially retain their coarse level values but extend over a smaller range (i.e., over one element). A mathematical explanation for this behavior indicates that the localized stress is due to the local imbalance (due to discretization error) in the applied shear loads. Thus to equilibrate the applied in-plane stresses on the edges a jump in element stress is required. The same behavior generally occurs when non-equal shear stresses are applied near the corner.

The solid sub-model, mesh and stresses are shown in Figure 23 and, the stress intensity linearization paths and corresponding linearized stresses extracted from the solid model are shown in Figure 24 and tabulated in Table 12. The limiting linearized stress in the solid sub-model is **2254 psi**, which, when compared against the one obtained in the shell sub-model (**3176 psi**) yields the stress reduction factor:  $2254/3176 = 0.71$ .

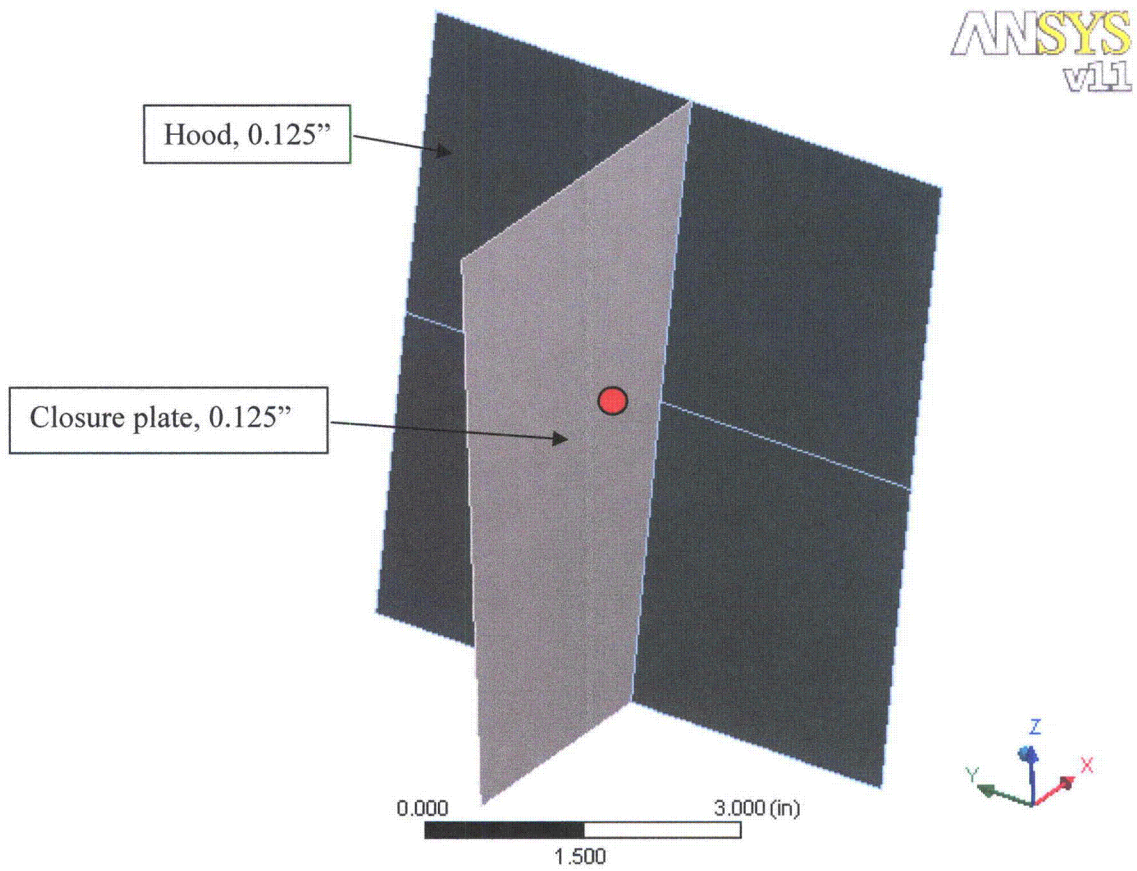


Figure 22a. Shell sub-model node 91605.

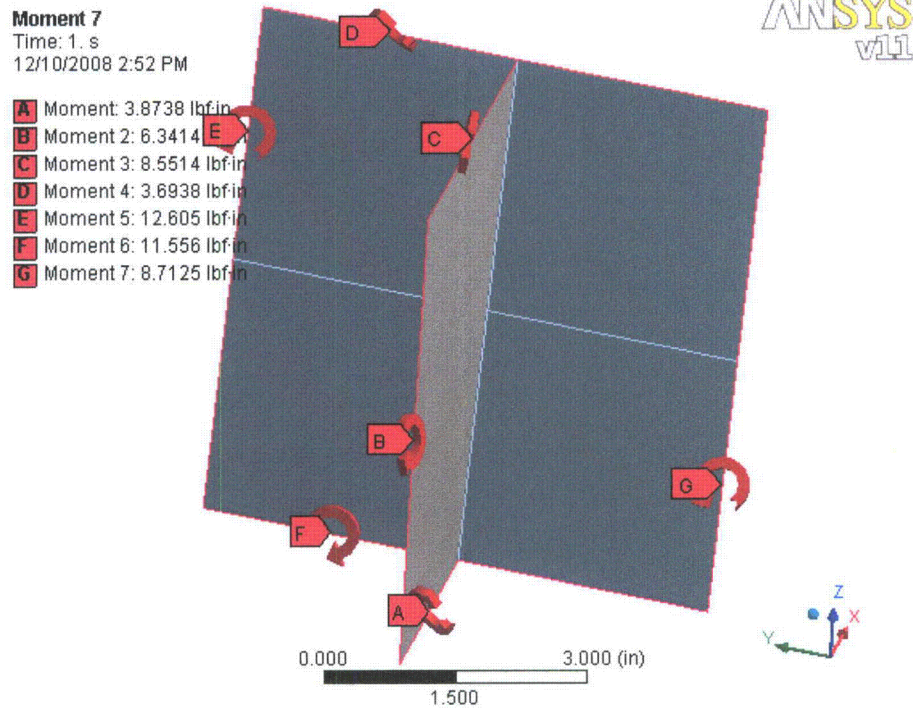
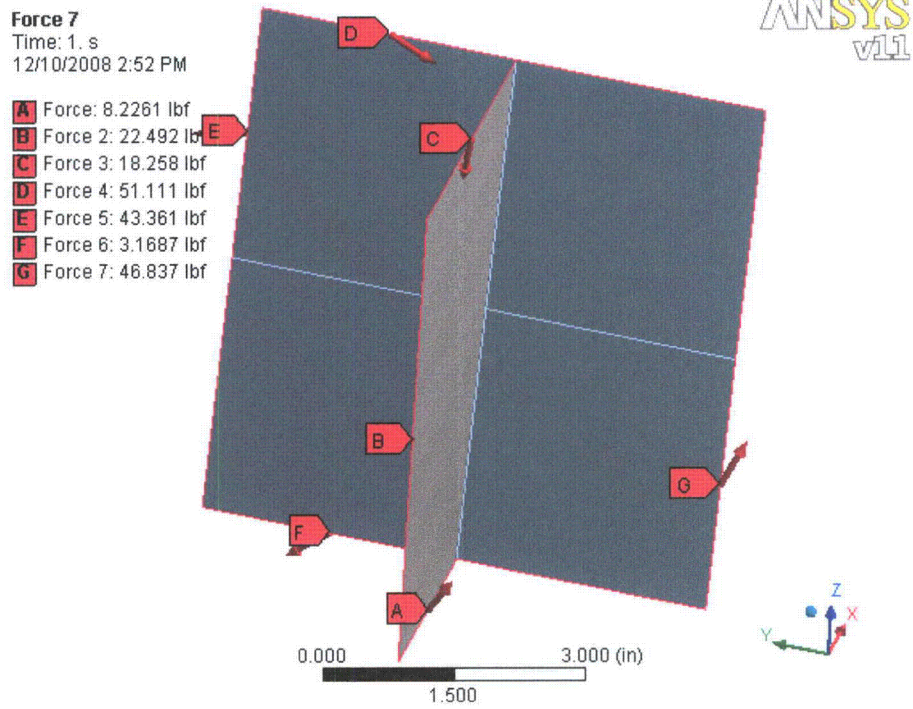


Figure 22b. Forces and moments.

**Stress Intensity**

Type: Stress Intensity - Top/Bottom  
Unit: psi  
Time: 1  
12/10/2008 2:56 PM

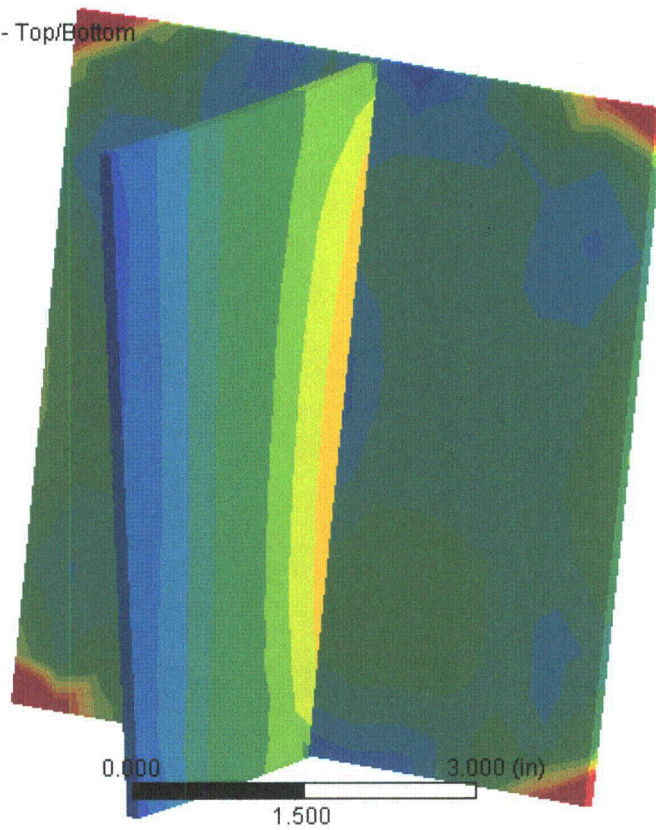
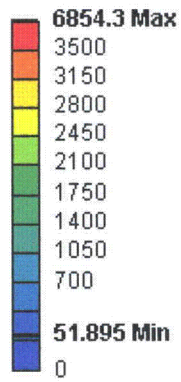


Figure 22c. Shell sub-model stress contours. Stress intensity: 3176 psi.

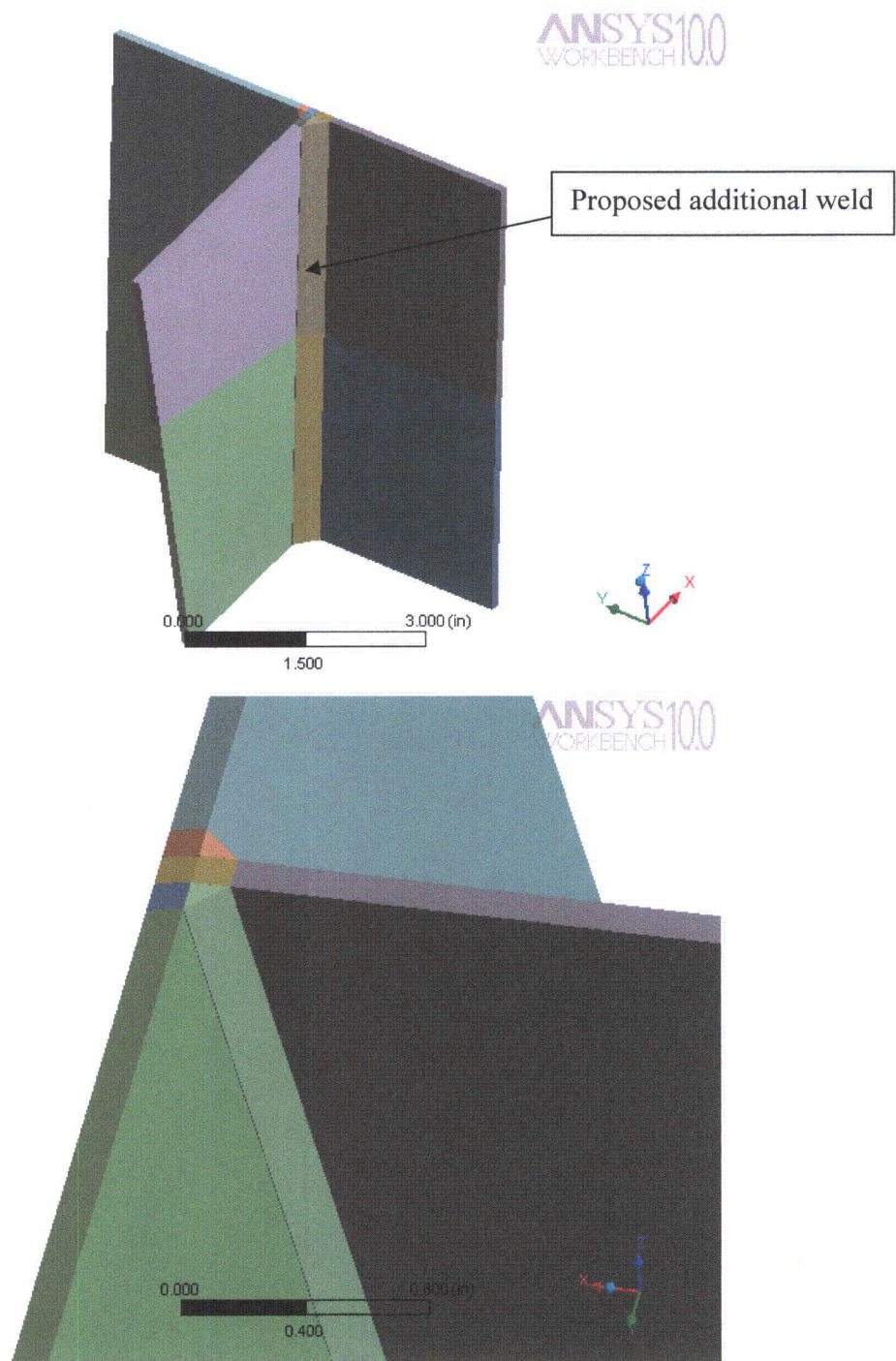


Figure 23a. Solid model geometry.

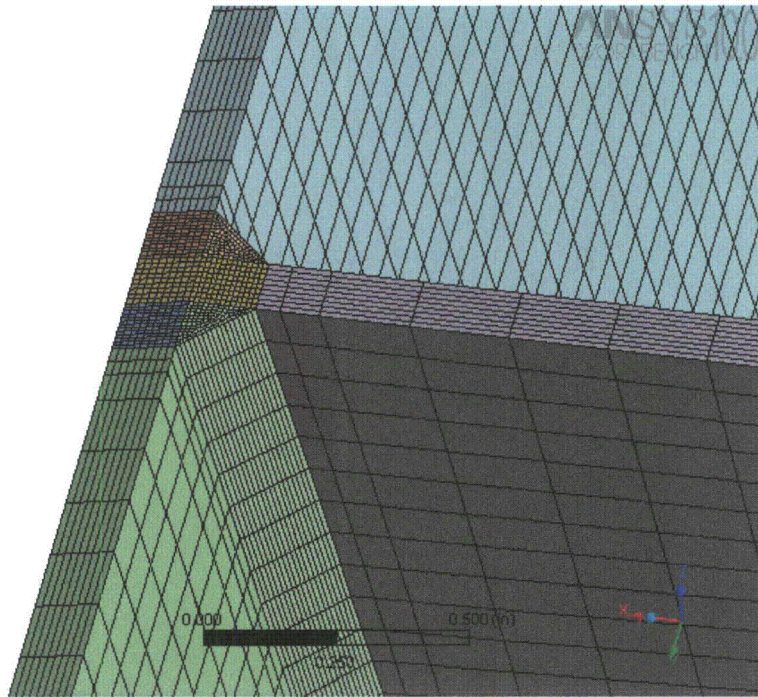


Figure 23b. Mesh overview.

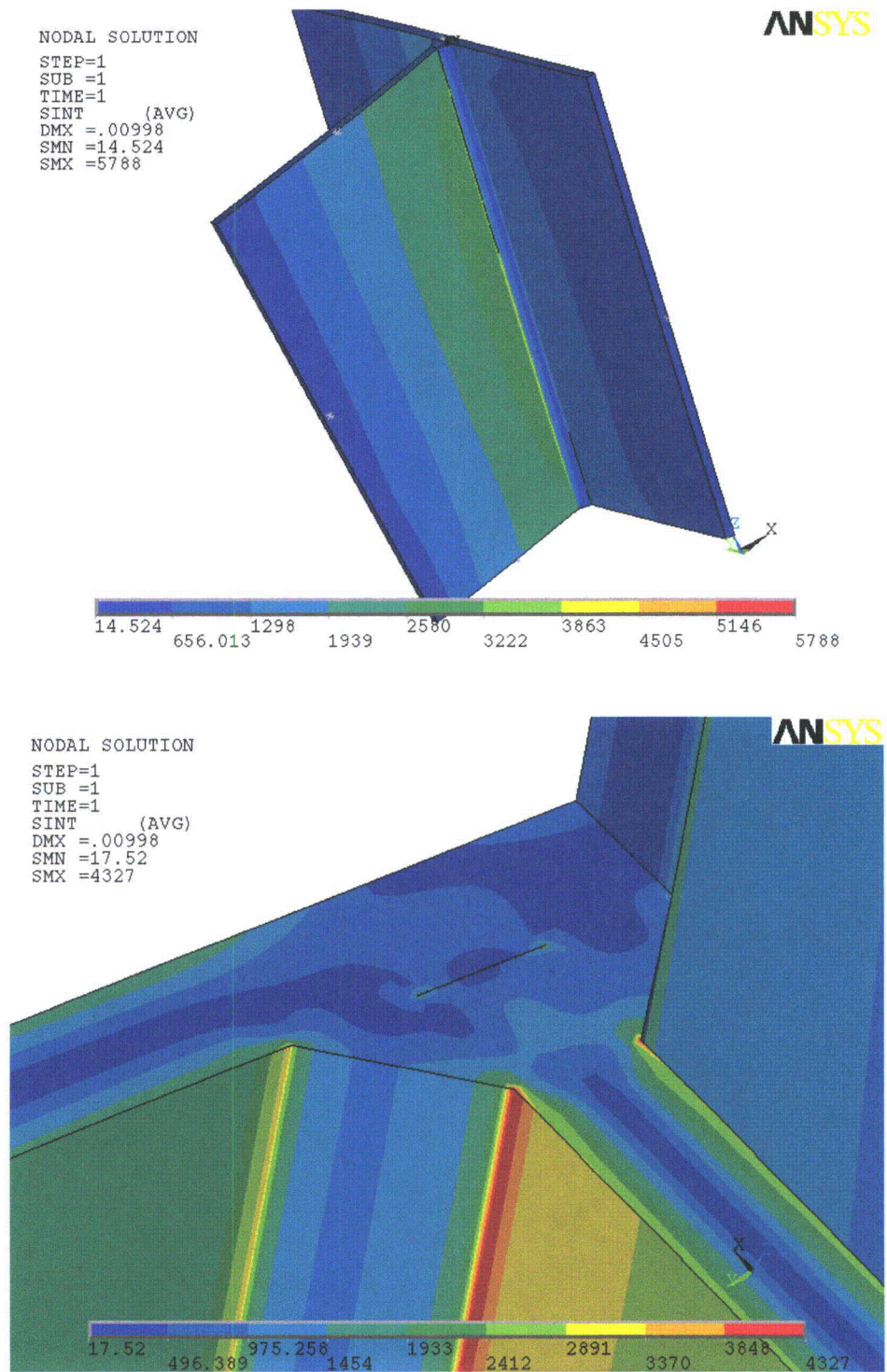


Figure 23c. Stress intensity contours (total) in solid sub-model. Part of structure is removed in the lower figure to show internal stress distribution.

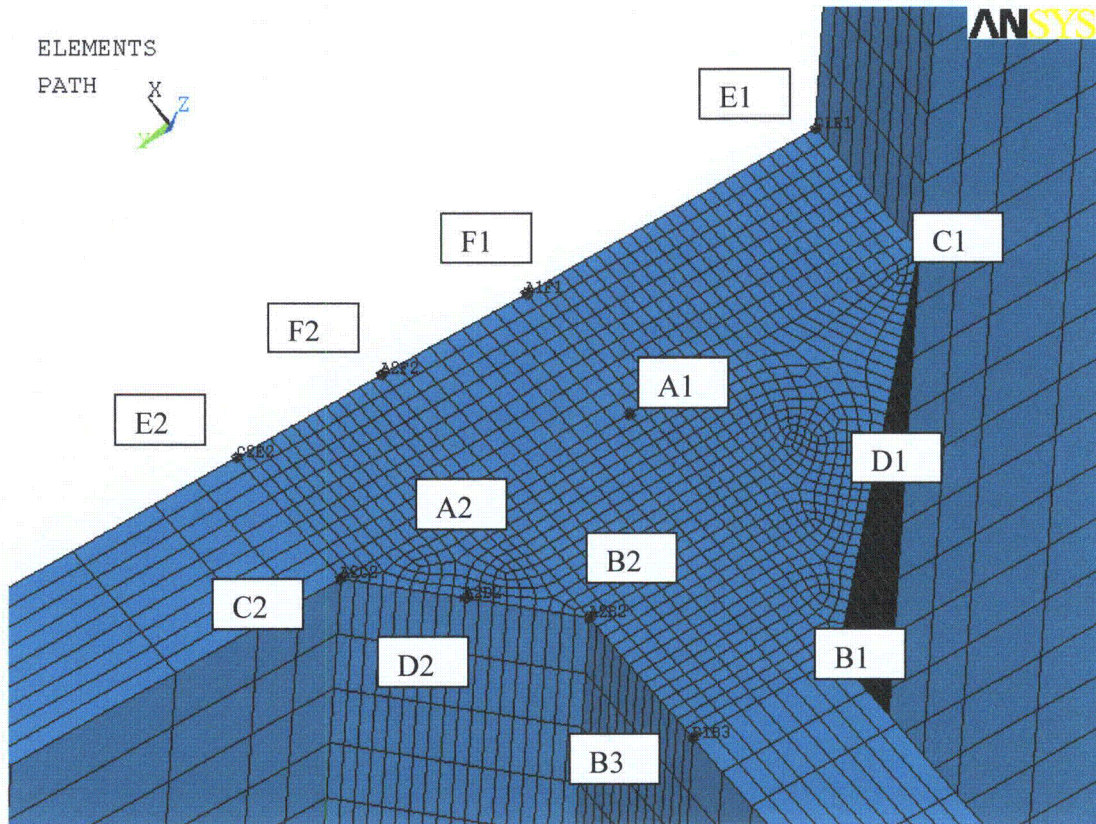


Figure 24. Linearization paths for sub-model node 91605.

Table 12. Linearized stresses along the linearization paths shown in Figure 24.

Path	Membrane + bending linearized stress intensity, psi
A1-B1	2254
A1-C1	1891
A1-D1	1261
A1-F1	822
C1-E1	1899
A2-B2	2170
A2-C2	1154
A2-D2	1160
A2-F2	867
C2-E2	930
B1-B2	2139

**Sub model node 95172.**

The sub-model for this node located at the top of the weld connecting the closure plate to the curved hood is shown in Figure 25a and again involves only two distinct components - the curved hood and closure plate. The extracted forces are shown in Figure 25b and the shell sub-model stress distribution is shown in Figure 25c with a maximum (i.e., the maximum taken over all components and surfaces – top, bottom and middle) stress intensity stress at the location of 3198 psi. The solid sub-model, mesh and stresses are shown in Figure 26 and, the stress intensity linearization paths on the original and added weld are shown in Figure 27. The corresponding linearized stresses extracted from the solid model are tabulated in Table 13. The limiting linearized stress in the solid sub-model is **2762 psi**. The corresponding value in the shell sub-model is **3198 psi** so that the stress reduction factor is  $2762/3198 = 0.86$ .

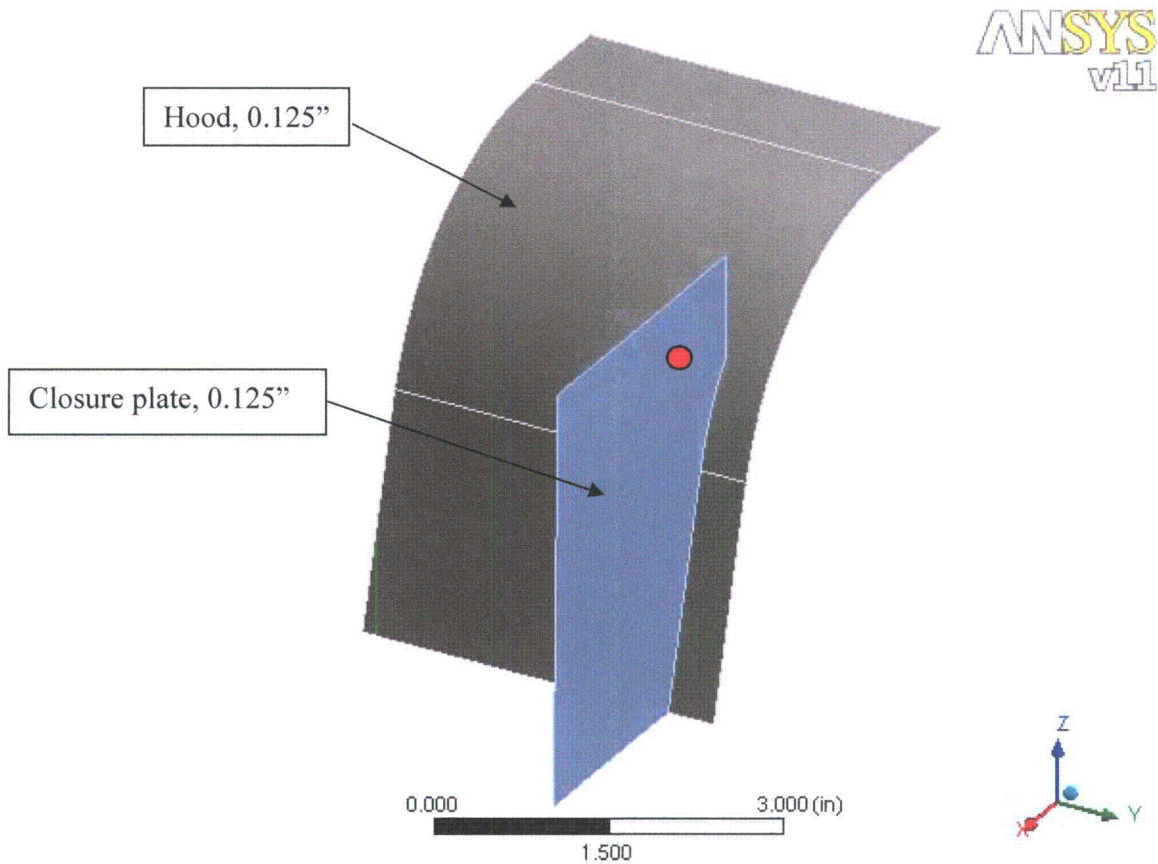
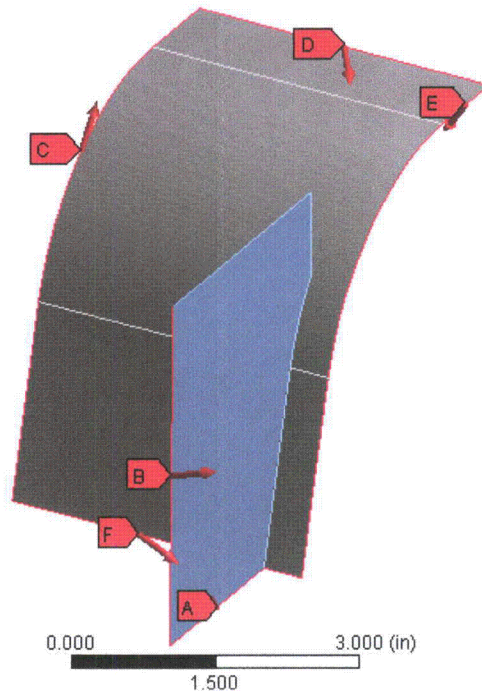


Figure 25a. Shell sub-model node 95172.

**Force 6**

Time: 1. s  
12/10/2008 10:33 PM

- A** Force: 4.3941 lbf
- B** Force 2: 13.957 lbf
- C** Force 3: 13.152 lbf
- D** Force 4: 5.8579 lbf
- E** Force 5: 12.614 lbf
- F** Force 6: 19.54 lbf



**Moment 6**

Time: 1. s  
12/10/2008 10:33 PM

- A** Moment: 3.3253 lbf·in
- B** Moment 2: 6.7324 lbf·in
- C** Moment 3: 38.492 lbf·in
- D** Moment 4: 4.9806 lbf·in
- E** Moment 5: 12.813 lbf·in
- F** Moment 6: 2.5859 lbf·in

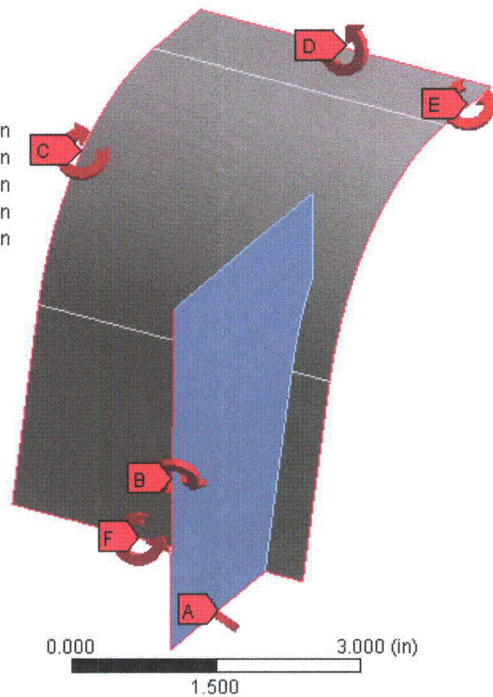


Figure 25b. Forces and moments.

**Stress Intensity**

Type: Stress Intensity - Top/Bottom  
Unit: psi  
Time: 1  
12/10/2008 10:42 PM

ANSYS  
v11

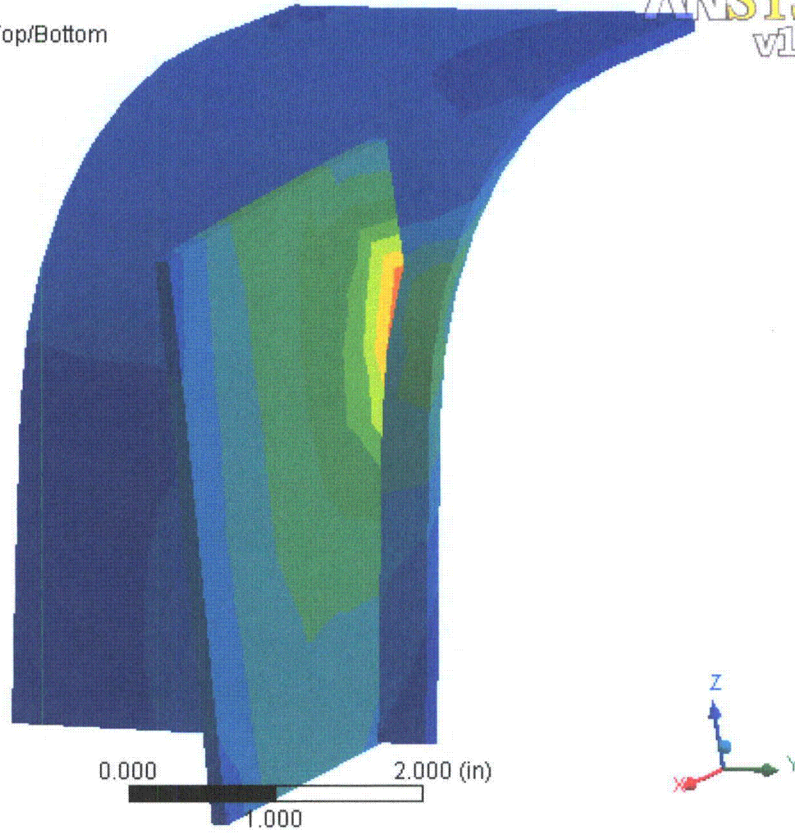
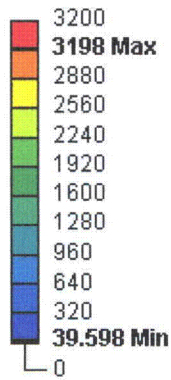


Figure 25c. Shell sub-model stress contours. Stress intensity: 3198 psi.

ANSYS100  
WORKBENCH

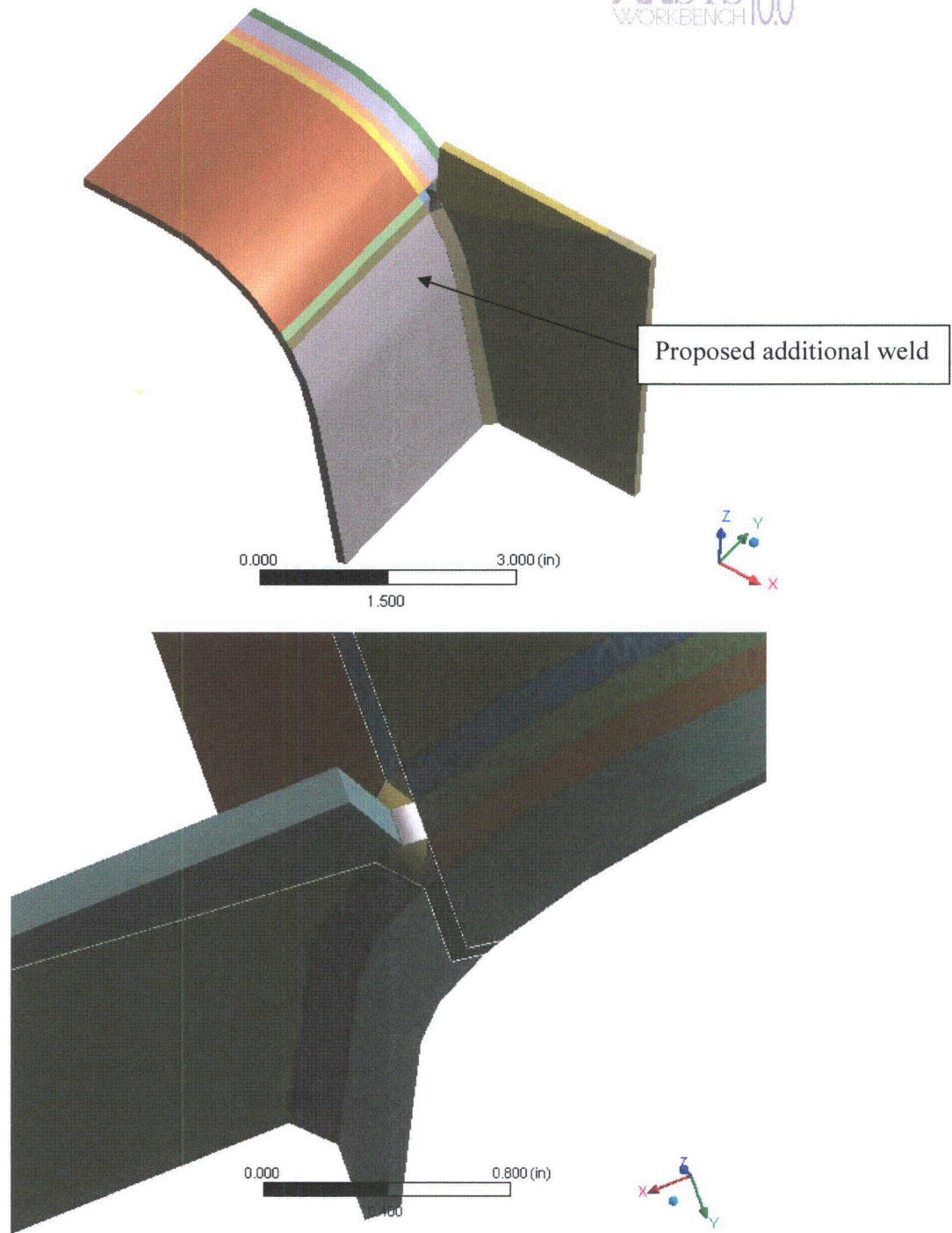


Figure 26a. Solid model geometry.

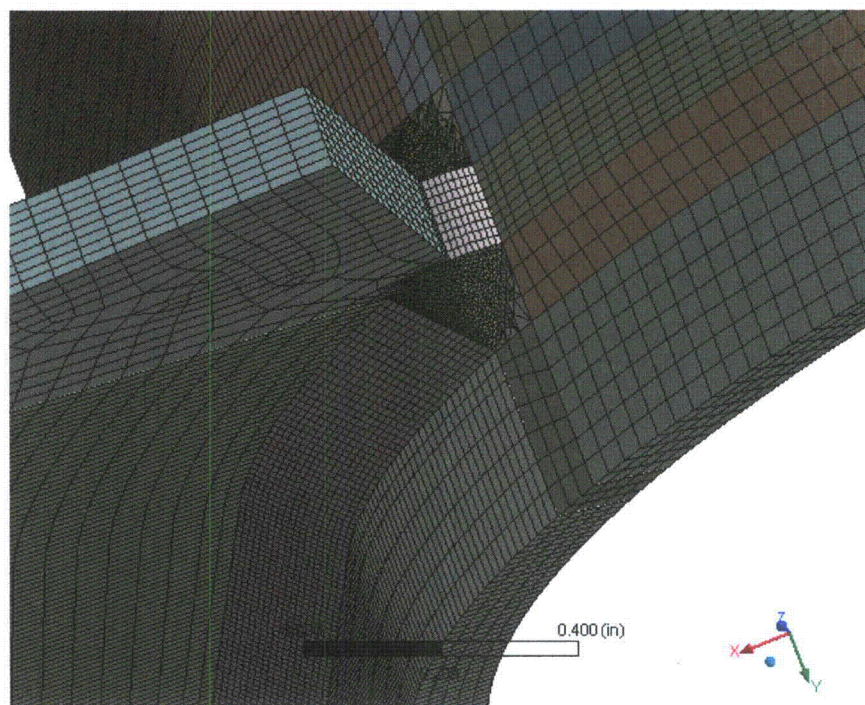


Figure 26b. Solid mesh.

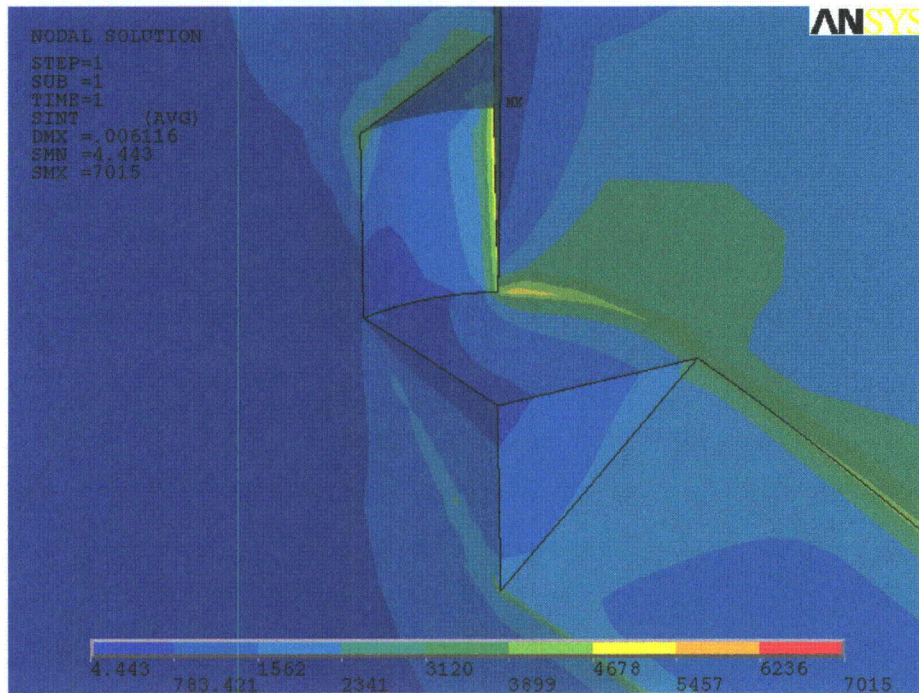
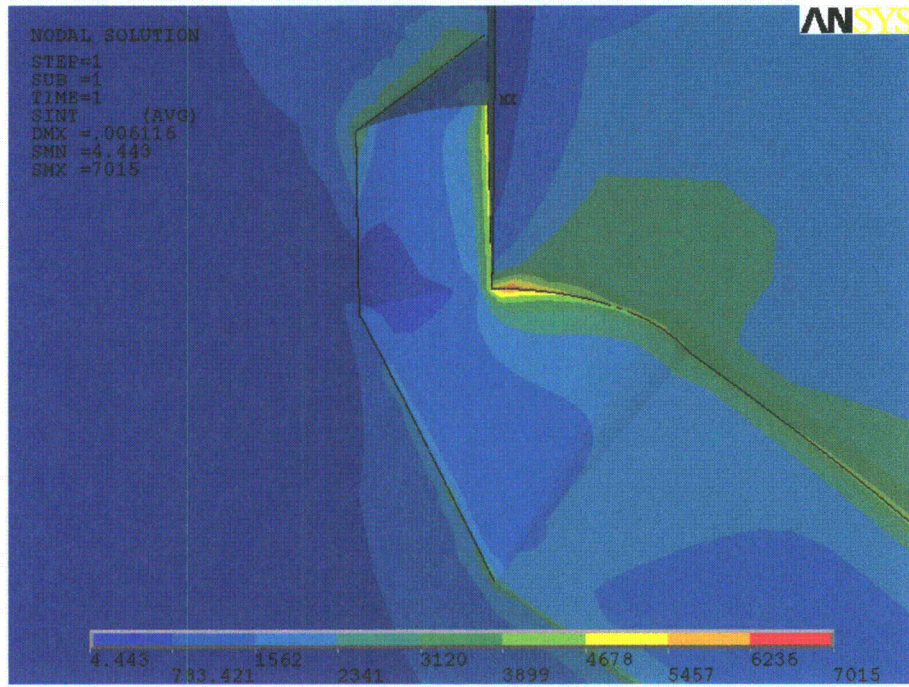


Figure 26c. Stress intensity contours (total) in solid sub-model.

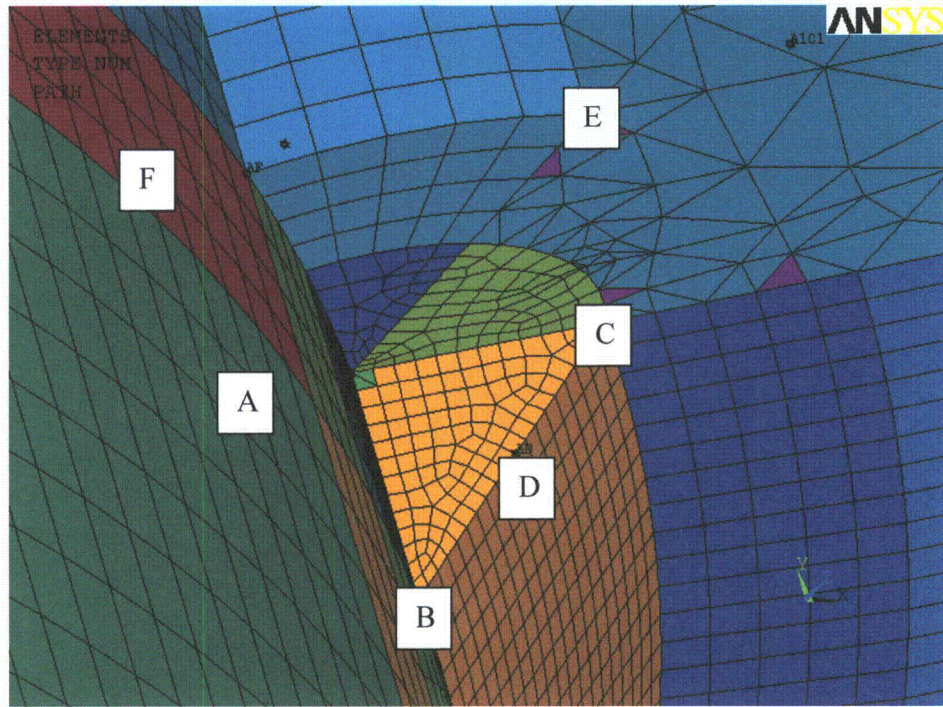


Figure 27a. Linearization paths at the original weld for sub-model node 95172.

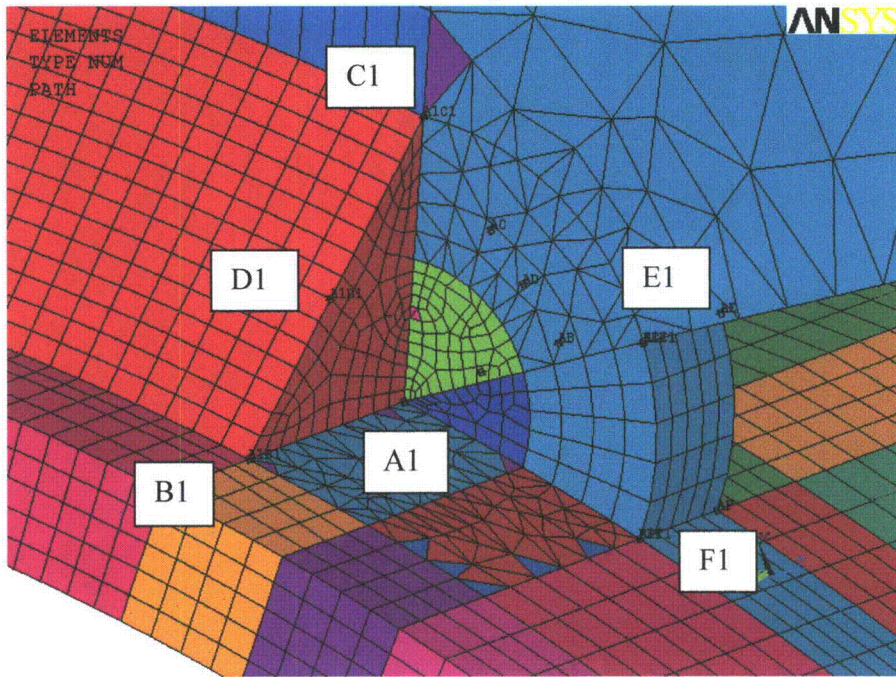


Figure 27b. Linearization paths at the additional weld for sub-model node 95172.

Table 13. Linearized stresses along the linearization paths shown in Figure 27.

Path	Membrane + bending linearized stress intensity, psi
AB	1910
AC	2437
AD	1696
AE	2421
AF	639
A1-B1	2002
A1-C1	2689
A1-D1	1837
A1-E1	2696
A1-F1	1598
C-C1	2762

### Sub model node 100327.

The final sub-model involving the closure plate is for a node on the vertical weld connecting the closure plate to the vane bank. It is located 13.5 inches below the top of the weld. The shell element-based sub-model is shown in Figure 28a and involves four components. The extracted forces are shown in Figure 28b and the shell sub-model stress distribution is shown in Figure 28c with a maximum stress intensity stress at the location of 2744 psi. The solid sub-model, mesh and stresses are shown in Figure 29 and, the stress intensity linearization paths depicted in Figure 30. The extracted linearized stresses are tabulated in Table 14 and show a limiting linearized stress in the solid sub-model of **2406 psi**. The stress reduction factor is  $2406/2744 = 0.88$ .

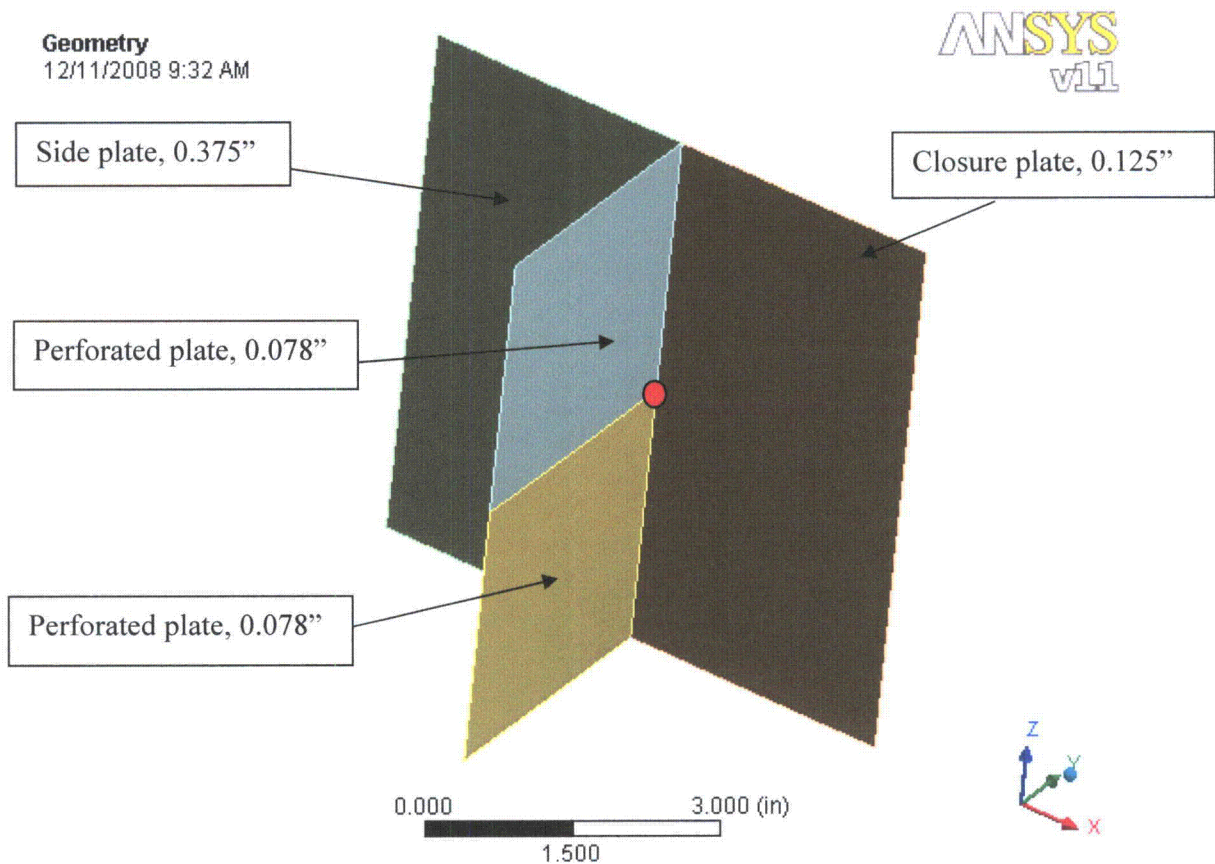
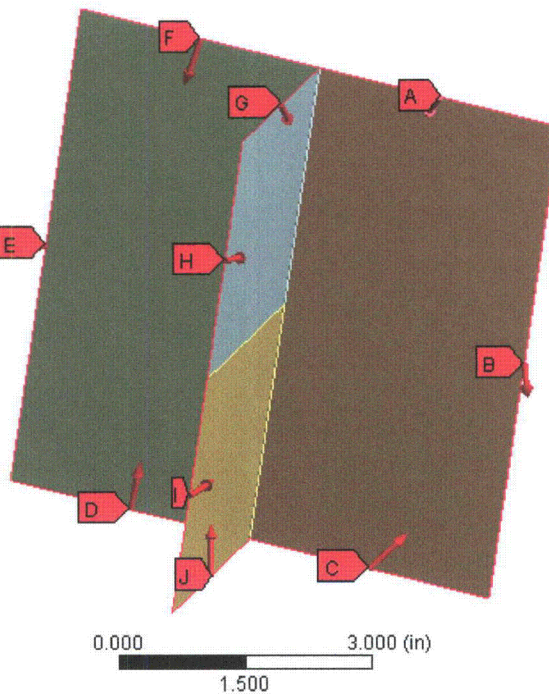


Figure 28a. Shell sub-model node 100327.

**Force 10**

Time: 1. s  
12/11/2008 9:44 AM

- A** Force: 2.6676 lbf
- B** Force 2: 9.5592 lbf
- C** Force 3: 4.0198 lbf
- D** Force 4: 7.6292 lbf
- E** Force 5: 14.618 lbf
- F** Force 6: 5.0388 lbf
- G** Force 7: 3.1685 lbf
- H** Force 8: 8.9608 lbf
- I** Force 9: 9.0228 lbf
- J** Force 10: 2.967 lbf



**Moment 10**

Time: 1. s  
12/11/2008 9:44 AM

- A** Moment: 2.7487 lbf-in
- B** Moment 2: 4.1118 lbf-in
- C** Moment 3: 2.8888 lbf-in
- D** Moment 4: 5.9596 lbf-in
- E** Moment 5: 22.463 lbf-in
- F** Moment 6: 5.067 lbf-in
- G** Moment 7: 1.2317 lbf-in
- H** Moment 8: 0.74244 lbf-in
- I** Moment 9: 0.41921 lbf-in
- J** Moment 10: 1.7222 lbf-in

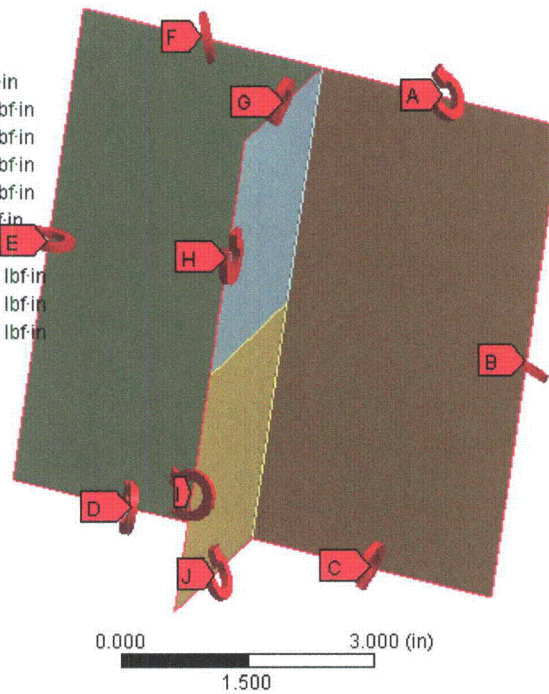


Figure 28b. Forces and moments.



**Stress Intensity**

Type: Stress Intensity - Top/Bottom

Unit: psi

Time: 1

12/11/2008 9:51 AM

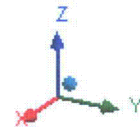
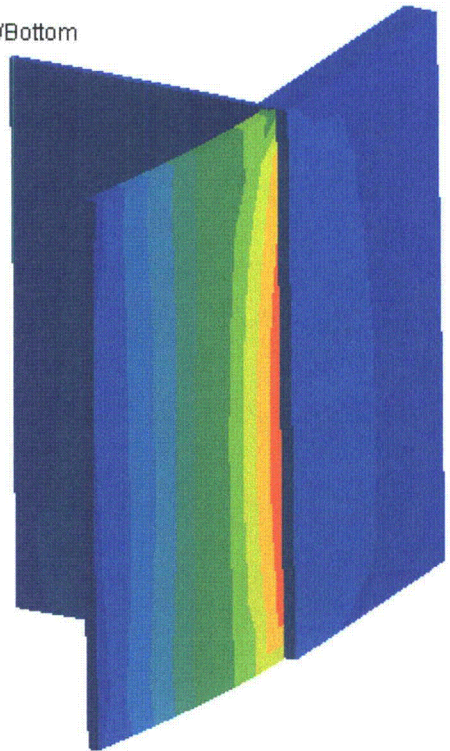
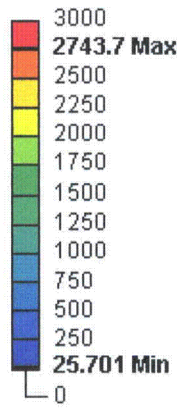


Figure 28c. Shell sub-model stress contours. Stress intensity: 2744 psi.

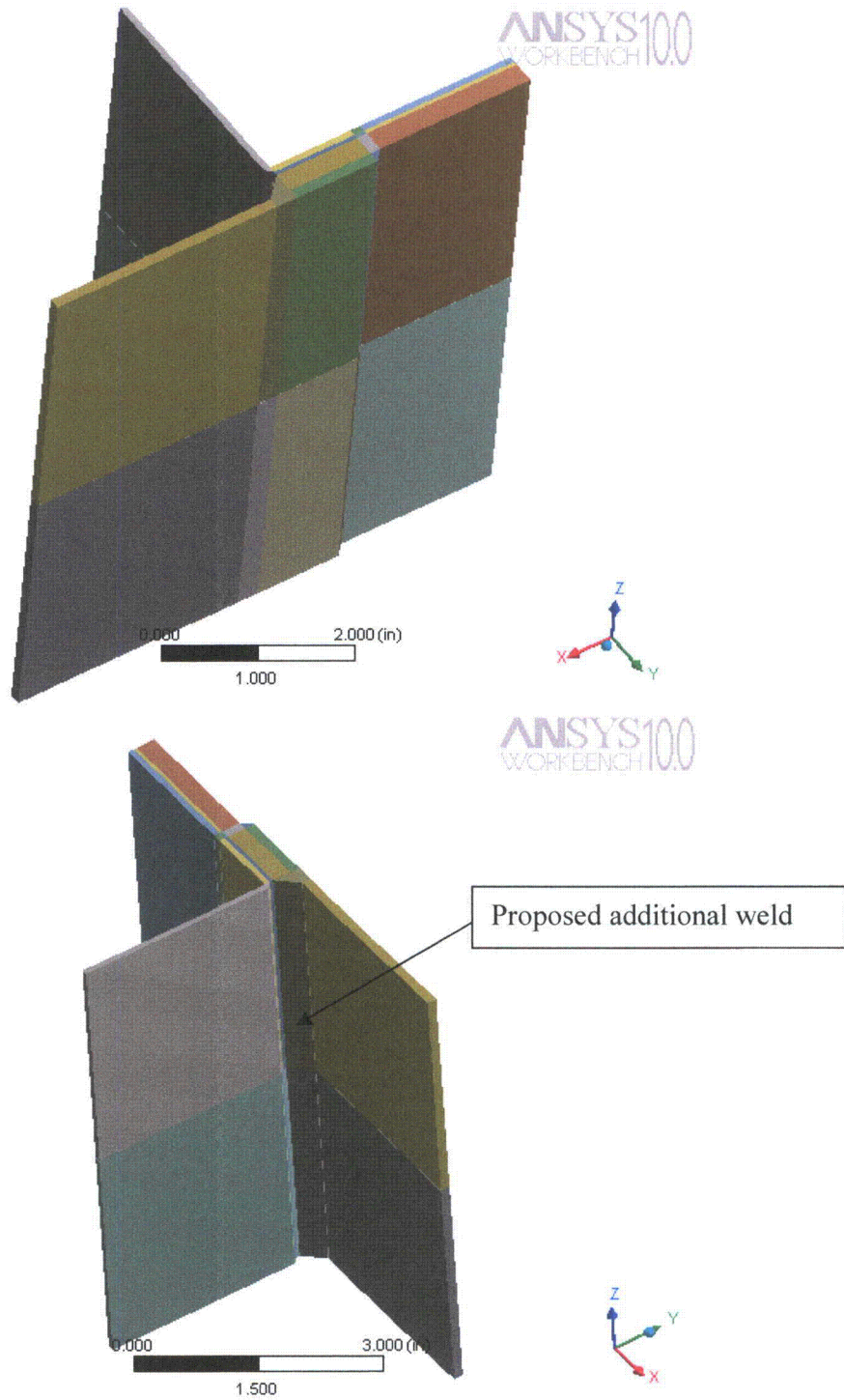


Figure 29a. Solid model geometry.

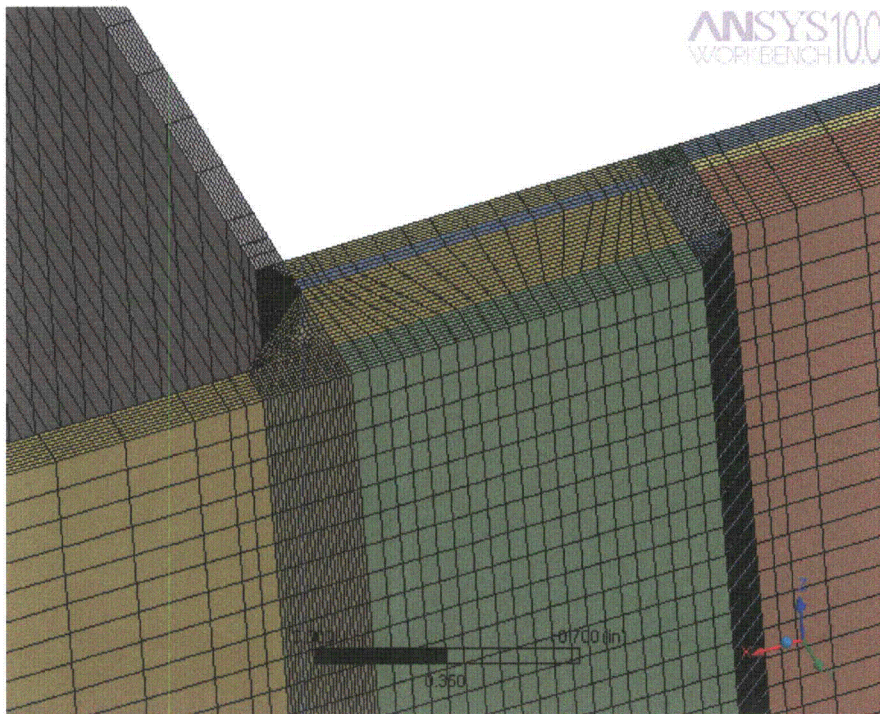
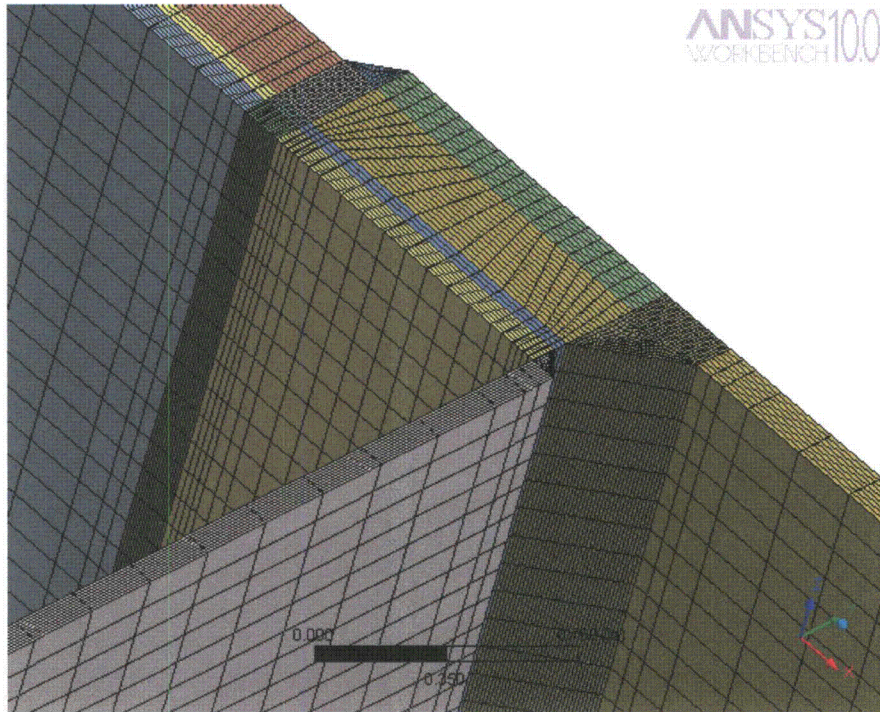


Figure 29b. Solid mesh. Mesh parameters: 567369 nodes, 133680 elements.

```
NODAL SOLUTION  
STEP=1  
SUB =1  
TIME=1  
SINT (AVG)  
DMX =.004133  
SMN =-1.847  
SMX =6458
```

ANSYS

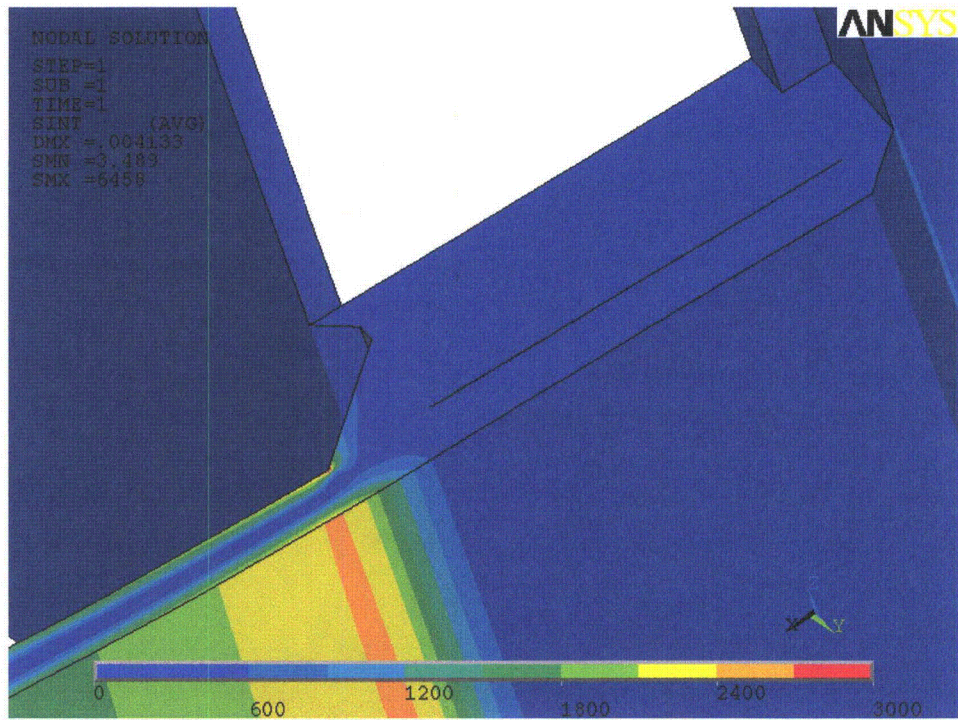
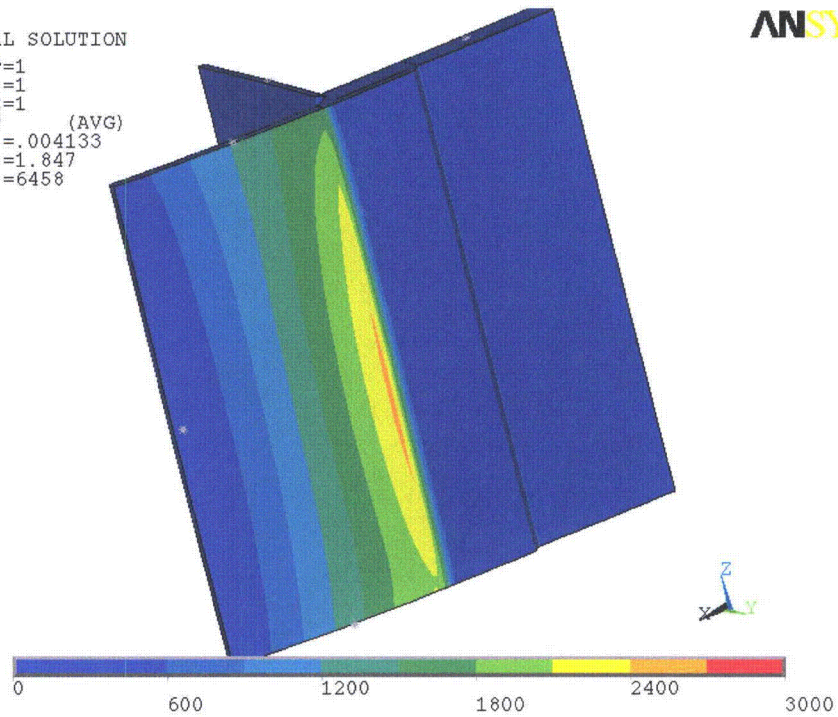


Figure 29c. Stress intensity contours (total) in solid sub-model. Parts of the structure removed to show internal stress distribution (bottom).

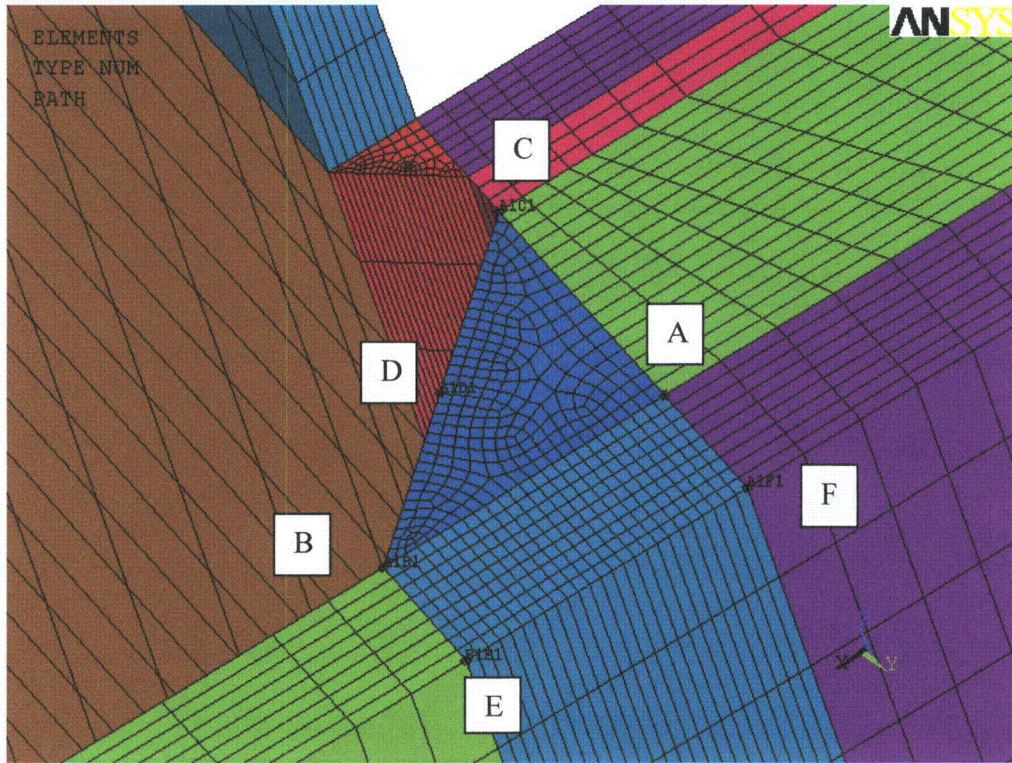


Figure 30. Linearization paths at the additional weld for sub-model node 100327.

Table 14. Linearized stresses along the linearization paths shown in Figure 30.

Path	Membrane + bending linearized stress intensity, psi
AB	1589
AC	439
AD	724
BE	2406
AF	488